SHIELDING EFFECT OF AC CONDUCTORS IN AC/DC HYBRID POWER TRANSMISSION

by

Hui Wang

A thesis
presented to the University of Manitoba
in partial fulfillment of the
requirements for the degree of
Master of Science
in
Electrical Engineering

Winnipeg, Manitoba

ISBN 0-315-63266-6

SHIELDING EFFECT OF AC CONDUCTORS IN AC/DC HYBRID POWER TRANSMISSION

BY

HUI WANG

A thesis submitted to the Faculty of Graduate Studies of the University of Manitoba in partial fulfillment of the requirements of the degree of

MASTER OF SCIENCE

I hereby declare that I am the sole author of this thesis.

I authorize the University of Manitoba to lend this thesis to other institutions or individuals for the purpose of scholarly research.

Hui Wang

I further authorize the University of Manitoba to reproduce this thesis by photocopying or by other means, in total or in part, at the request of other institutions or individuals for the purpose of scholarly research.

Hui Wang

The University of Manitoba requires the signatures of all persons using or photocopying this thesis. Please sign below, and give address and date.

ABSTRACT

The increasing requirement for the power transfer capability has raised the possibility of dc transmission lines operating on an existing ac transmission corridor. Corona effects in such hybrid ac/dc lines become much more complicated due to the interaction between the ac and dc fields. This thesis presents a method to investigate the ionized field of such hybrid ac/dc lines and evaluate the shielding effect of the ac conductors on the electric field intensity and the ionic dc current density at ground level from the point of view of environmental impact. The method is based on an iterative finite element procedure to solve the time invariant ionized field.

A comparison between the calculated and experimental results for a laboratory line is presented. The calculated values of the current density at ground level agree satisfactorily with the experimental results.

The calculated data, including the ground level lateral profiles of the electric field intensity and the current density for practical hybrid transmission line configurations, are also given in this thesis. For further discussion of the shielding effect of the ac conductors on the electric environment in the hybrid ac/dc lines, the calculated data for a bipolar dc transmission line configuration are presented as well. The results show that with a proper ac line arrangement, the hybrid ac/dc line geometries have the advantage of reducing the ionized field and the current density at ground level.

ACKNOWLEDGEMENTS

The author would like to express deep gratitude to Professor I. M. R. Ciric and Professor M. R. Raghuveer for their invaluable guidance and support through the course of this work.

The author would also like to acknowledge the financial support from Manitoba Hydro and the National Science and Engineering Research Council.

TABLE OF CONTENTS

Page

Page

LIST OF FIGURES

Figure Page

Figure Page

LIST OF TABLES

Chapter1
INTRODUCTION

With the increasing demand for the supply of electric power, the possibility of using hybrid ac/dc transmission lines has been sought [1,2,3,4,5]. A hybrid ac/dc transmission line is a transmission line with both ac and dc conductors on the same tower or adjacent towers sharing the same right-of-way (ROW). It may be created by adding a bipolar dc transmission line to an existing three phase ac transmission system. Thus, a hybrid ac/dc system will not only increase the power transfer capacity of the existing transmission corridor, but also improve the stability and controllability of the ac network [1, 2].

It is well-known that the corona effect of a HVDC transmission line requires serious consideration due to the power loss (PL), radio interference (RI), audible noise (AN), and the electrification of isolated objects or human bodies associated with it [6,7]. In hybrid ac/dc lines, the interaction of ac and dc fields affects the corona activity, making the ionized field problem even more complicated. Thus, a thorough study of the ionized field of hybrid ac/dc lines is needed before they are put into practical use.

1.1 PHYSICAL CHARACTERISTICS OF CORONA

Corona is a self-sustained partial breakdown of air in the nonuniform field surrounding the conductor of a power transmission line. In positive dc corona, it is usually assumed that an electron starts an avalanche from the edge of the ionization zone where the field intensity is sufficiently high that the ionization coefficient is greater than the coefficient of electron attachment. A series of successive electron avalanches is developed towards the conductor surface, under the combined influence of its own space charge and the applied electric field. Positive ions and excited molecules are produced due to the ionizing collisions and are left behind by the electrons. The excited molecules reverting to their stable states give up their energy in the form of photon radiation. Therefore, the electrons necessary for maintaining the self-sustained discharge are provided by the photonization of gas molecules. As a result, the electrons are neutralized on the conductor and the positive ions drift away from the conductor spreading all over the inter-electrode region. Similarly, a negative dc corona results in negative ions filling the entire inter-electrode region.

In the case of bipolar dc transmission line in corona, the ions generated by each conductor drift either to the conductor of opposite polarity, or to the ground. Thus, ions of either positive or negative polarity fill the regions between each conductor and ground, and ions of both polarities are mixed in the region between the two conductors.

In the case of ac transmission line in corona, however, the space charge created by corona is constrained to the vicinity of the conductors because of the periodic reversal

of the applied voltage. Consequently, ac corona has negligible impact on the electrical environment at ground level.

1.2 OBJECTIVE OF THE THESIS

As mentioned earlier, the creation and movement of the space charges cause power loss (PL), audible noise (AN), and radio and television (RI & TVI) interference. Another very important effect of corona is the environmental impact. Any object located under transmission lines intercepts the ion flow between the conductors and the ground. If the object is perfectly insulated from the ground, the magnitude of its potential above ground gradually increases until it approaches the equilibrium space potential or until the insulation breaks down. In practice, the potential to which the object is raised will be limited by its insulation resistance to ground. If a grounded person touches the object, he may receive an initial carpet-type shock of extremely short duration followed by a small steady current. Similar induction effects are also produced when a well-insulated person located under the line touches a grounded object. A well-grounded person standing under a dc line will also experience a steady flow of very small current. Thus, the electrification of isolated objects or human bodies by space charges is one of the most important factors in designing overhead power transmission lines. The electric field intensity (E) and the ion current density (J) on the ground are significant environmental factors related to the biological effects. To study these problems, the electric field distribution distorted by the ion space charge (ρ) flowing from dc conductors must be calculated.

The aim of this thesis is to discuss such a computational procedure for hybrid ac/dc transmission lines. The electric quantities (E, ρ, J) at ground level have been calculated for different line geometries. The effect of ac conductor voltages and the shielding effect of ac conductors on the dc corona activities at ground level have also been investigated.

These studies are based on a numerical solution for the ionized field by an iterative Finite Element (FE) procedure. Since the ac corona has negligible impact on the electrical environment and a prohibitively large computational effort is required to analyze the time varying ionized field, all solutions for corona on hybrid ac/dc lines are based on computations for unipolar dc corona.

1.3 LINE CONFIGURATIONS

Five line geometries are analyzed to study the arrangement and the shielding effect of the ac conductors.

The first is a laboratory line consisting of a positive dc conductor directly above an ac conductor, as shown in Figure 1.1

The second geometry is based on the Manitoba Hydro Gulfport power line with a bipolar dc transmission line replacing the ground wires of a three phase ac line.

The third geometry is the same as the second one except that the dc line is situated at a greater height.

The fourth geometry is also similar to the second one except that the outer phases of the ac lines (phases A & C) are situated further away from the center phase (phase B).

Figure 1.2 shows the line configuration for Geometries 2, 3, and 4.

The fifth geometry is again the same as the second one, but with the ac conductors removed as shown in Figure 1.3, i.e., Geometry 5 is a bipolar dc system for comparing the shielding effect of ac conductors in hybrid line configurations.

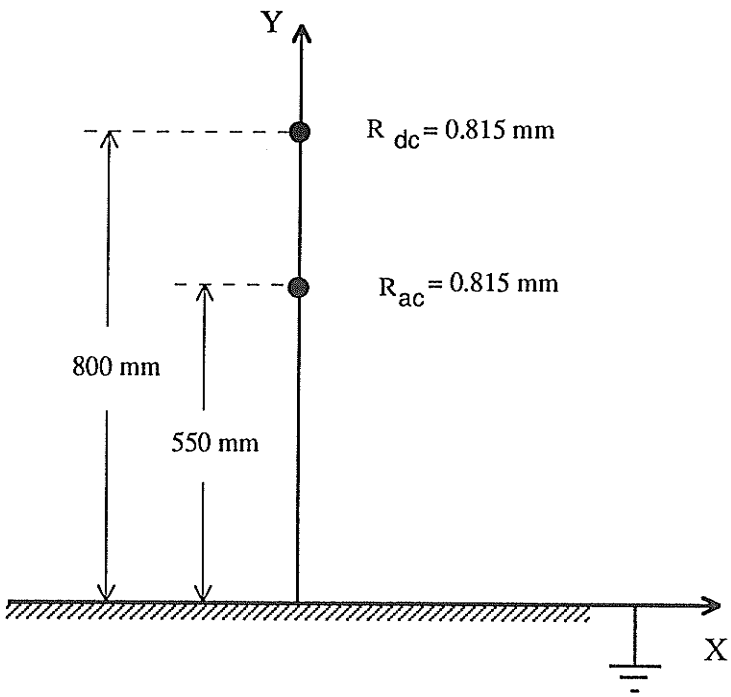

Figure 1.1: *Geometry 1, Laboratory Line*

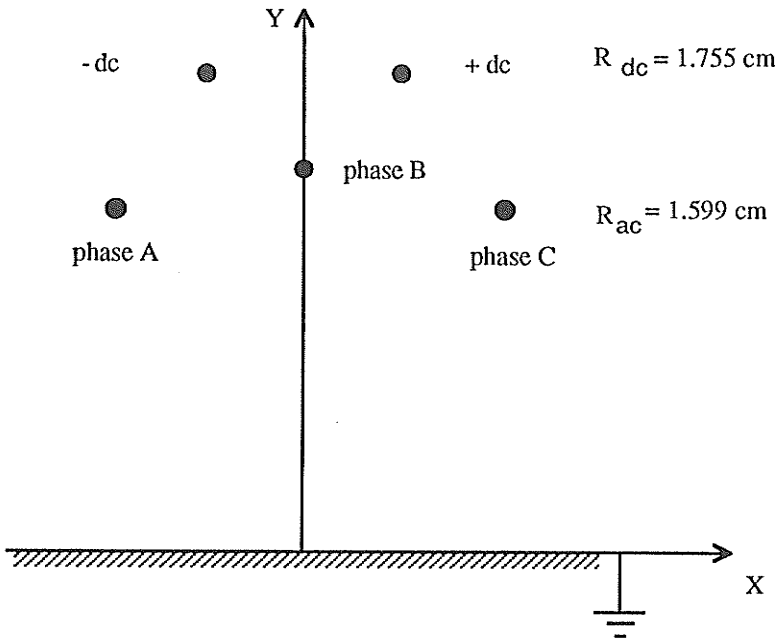

Figure 1.2: *Geometry 2, 3, and 4*

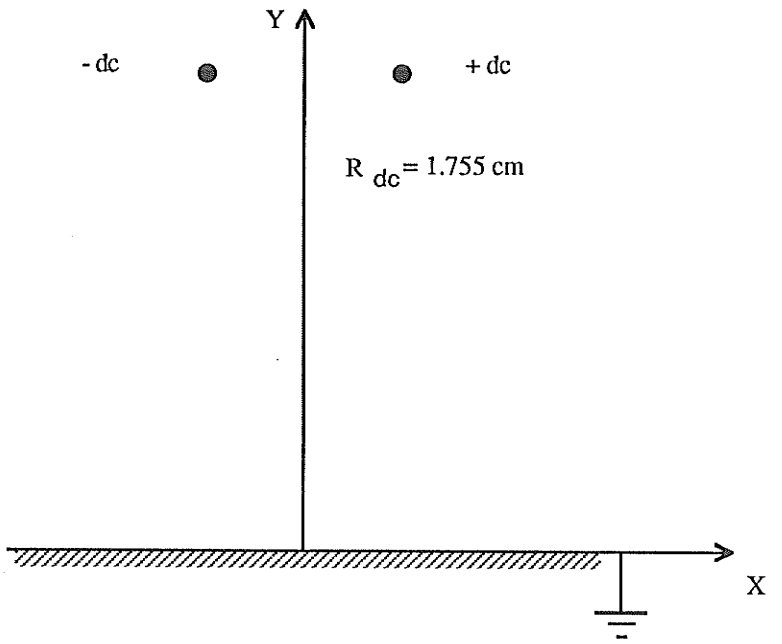

Figure 1.3: *Geometry 5*

The experimental results giving the ionic current density at ground level are available for the laboratory line (Geometry 1) with the dc applied voltage $V_{dc} = 60$ kV and the ac applied voltages of root mean square (RMS) values $V_{ac} = 0$, 10 kV, 20 kV, and 25 kV, respectively [5]. The computational results will be discussed with the same applied voltages in order to compare them with the available experimental results.

For Geometries 2 to 5, the computational results are based on the dc applied voltage $V_{dc} = \pm 300$ kV and the ac voltage zero.

Table 1.1 shows the line dimensions for these geometries (Geometries 2 to 5).

Table 1.1: *Dimensions for Various Configurations*

Conductor		-dc	+dc	phase A	phase B	phase C
Geometry 2	x(m)	-4.57	4.57	-5.49	0.0	5.49
	y(m)	16.34	16.34	12.38	14.20	12.38
Geometry 3	x(m)	-4.57	4.57	-5.49	0.0	5.49
	y(m)	17.34	17.34	12.38	14.20	12.38
Geometry 4	x(m)	-4.57	4.57	-6.49	0.0	6.49
	y(m)	16.34	16.34	12.38	14.20	12.38
Geometry 5	x(m)	-4.57	4.57	—	—	—
	y(m)	16.34	16.34	—	—	—

Chapter 2
LITERATURE REVIEW

2.1 ANALYSIS OF DC CORONA

2.1.1 Equations and Assumptions

As mentioned in Chapter 1, unipolar dc corona is characterized by a steady flow of ions from coronating conductors with the same polarity as the applied voltages. The flow of ions, i.e., the ionic current density **J**, is determined by the local electric field intensity **E**. This quantity is in turn governed by both the potentials applied to the conductors and the special distribution of the corona-generated space charge density ρ. This mutual interaction between **E** and ρ for an unipolar dc corona is described by the following equations:

$$\nabla \cdot \mathbf{E} = \frac{\rho}{\varepsilon_o} \tag{2.1}$$

$$\nabla \cdot \mathbf{J} = 0 \tag{2.2}$$

$$\mathbf{J} = k\rho\mathbf{E} \tag{2.3}$$

$$\mathbf{E} = -\nabla\Phi \tag{2.4}$$

Equation (2.1) is Gauss's law, where ε_o is the permittivity of free space. Equation (2.2) is the continuity equation for the current density **J**. Equation (2.3) is the relation between **E** and **J**, where k is the mobility of ions. Equation (2.4) is the electric field intensity **E** in terms of the potential Φ.

Combining Equations (2.1) - (2.3), the ionized electric field is described by the following equation,

$$\mathbf{E}\cdot \nabla (\nabla\cdot \mathbf{E}) + (\nabla\cdot \mathbf{E})^2 = 0 \tag{2.5}$$

Or, using Equation (2.4), in terms of potential,

$$\nabla\cdot (\nabla\Phi\nabla^2\Phi) = 0 \tag{2.6}$$

Equations (2.5) and (2.6) are the general equations describing a unipolar ionized field. They are nonlinear third-order partial differential equations and there is no known method available for solving them for a general case. Some basic assumptions are necessary in order to make the solution of these equations possible. The following are the commonly used assumptions and simplifications [8]:

1. Ionic mobilities are constant, independent of the electric field intensity.

2. Mobilities of positive and negative ions are equal, and the corona onset voltage for positive and negative cases are the same for the bipolar case.

3. Diffusion of ions is neglected.

4. The effect of wind on space charge distribution is not considered.

5. The thickness of the ionization layer around the conductors in corona is assumed to be insignificant in comparison with other geometric parameters.

6. An equivalent steady state is assumed (i.e. temporal variations are neglected).

The above six assumptions have been well justified in literature. The problem is still too complex to solve even with these simplifications. Some further approximations are needed, which are different in different solution methods.

2.1.2 Review of Methods of Calculation

As mentioned above, Equation (2.6) is a nonlinear third-order partial differential equation. Thus, three boundary conditions are needed to solve the problem uniquely. However, only the potentials on the conductors and at ground are known precisely. A third boundary condition must be added to the coronating conductors. The choice of the third boundary condition varies with different solution methods.

Townsend [9] was the first to solve analytically for the ionized field in a coaxial cylindrical configuration, where due to the cylindrical symmetry, the unipolar ionized

field problem is reduced to a one dimensional problem. In his analysis, Townsend used the value of the electric field intensity on the surface of the coronating conductor as the third boundary condition, which is known as the Kaptzov's assumption. It states that the magnitude of the electric field intensity at the coronating conductor surface remains constant at its onset value regardless of the level of the applied voltage. It can be expressed as,

$$\left| \frac{d\Phi}{dn} \right| = E_o \tag{2.7}$$

where E_o is the value of the electric field intensity on the surface of the conductor at the onset of corona; n is the outward unit norm of the coronating conductor.

Deutsch [10] extended the analysis of unipolar ionized field to the two dimensional problem of a cylindrical conductor above an infinite ground plane. The basic assumption made by Deutsch is that space charge affects only the magnitude but not the direction of the electric field, which is now known as Deutsch's assumption. Thus, the two dimensional ionized field problem is reduced to a one dimensional problem again. He also assumed that the space charge density in the electrode space is constant and the field at the electrode not in corona is unaffected by the space charge. These are valid only for vanishingly small corona currents.

Popkov [11,12] proposed an improved analysis for the conductor-plane geometry by retaining Deutsch's and Kaptzov's assumptions. In addition, he introduced an additional assumption regarding the distribution of the corona current on ground plane. Based on laboratory measurements and Townsend's work for the concentric

cylinder case, Popkov presented a semi-empirical expression of the voltage-current relationship for the conductor-plane geometry, assuming that the conductor-plane configuration can be approximated by an equivalent cylindrical system.

A method of analyzing both unipolar and bipolar DC ionized fields has been proposed by Maruvada and Janischewskyj [13,14] by employing Deutsch's and Kaptzov's assumptions. They adopted the concept of iterations, originally suggested by Felici [15], and developed an algorithm applicable for corona computations on practical HVDC transmission lines.

A detailed investigation of the mathematical aspects of the DC ionized fields has been carried out by Atten [16]. He proved that the problem is "properly posed" if the third boundary condition is chosen to be the value of charge density on the coronating conductor. By assuming that the charge distribution around the coronating conductor surface was known, Atten developed a finite difference method of solving unipolar DC ionized fields without adopting Deutsch's assumption. However, accurate determination of the space charge distribution beforehand is impossible in practical cases [13].

Some researchers have employed the charge density as the third boundary condition. Takuma et al. [17] assumed a constant charge density on the conductor surface. The value of the charge density was determined by using an iterative procedure which matched the calculated current with the corresponding measured one. But the assumption of constant charge density is not realistic itself, especially for the case of bundled conductors where the charge density shows a significant change around the periphery of subconductors [18].

In order to study the effects of space charges on RI, Sunaga et al. [19] proposed a higher order boundary condition described by an empirical relation of the ion current density (J) with the surface field intensity (E) on the conductor, $J = b \exp(a E)$, in addition to Deutsch's assumption. But a lot of experimental work has to be done in order to determine the empirical constants a and b.

Khalifa et al. [20] replaced Kaptzov boundary condition by using the space charge distribution on the surface of the coronating conductor as the third boundary condition. They assumed the ion charge density at each point on the conductor surface to be proportional to the average ion density inside the head of the avalanche developed at the same point. But in their analysis, the space-charge-free field was used in the avalanche calculations.

Gela and Janischewskyj [21] proposed a Finite Element Method (FEM), for the first time, to solve the ionized field in a simple coaxial cylindrical configuration without recourse to Deutsch's assumption, but to Kaptzov's assumption.

Abdel - Salam et al. [22] claimed that they applied FEM to analyze the unipolar dc ionized field without retaining both Deutsch's and Kaptzov's assumptions by using the known field quantities along the axis of symmetry as the third boundary condition. Their results showed a decrease of the surface field intensity of the conductor with the applied voltage in the same manner as reported by others [19, 23, 24, 25].

The charge simulation method (CSM) has been applied by many researchers for

calculating the space-charge-free field [26, 27]. For the first time, Horenstein [28] has applied CSM to approximate the electric field and space charge around a single conductor in corona and to compute the V-I relationship for the discharge. More recently, Qin et al. [29] claimed that they had developed an iterative numerical method for accurate calculation of the ionized field quantities associated with HVDC bipolar lines. The computational procedure employed the CSM for calculating the ionized field and a weighted residual method for calculating the space charge densities. Very recently, Abdel - Salam and Abdel - Scattar [30] have applied CSM for modelling the V-I characteristics of corona for unipolar bundled transmission lines. Their main concern is to remove Deutsch's assumption in their analysis. By comparing their computational results with the experimental ones, they conclude that their proposed method (CSM) is more accurate than the previous iterative method [13] .

2.2 ANALYSIS OF CORONA ON HYBRID AC / DC LINES

Chartier et al. [1] were the first who published the analysis of corona on hybrid ac/dc lines. In their studies, they calculated the space-charge-free fields on the conductor surfaces and at the ground level of a hybrid ac/dc system. They also obtained the important corona performance parameters such as RI and AN.

Maruvada and Drogi [3] were the first who analyzed the effects of space charge on the ionized field of hybrid ac/dc lines operating on both a same tower as well as on two adjacent towers. In their approach, they employed Deutsch's assumption and considered that the presence of the alternating field component has negligible influence on the ion trajectories. This allowed them to assume the ac conductors to be at zero

potential, and thus reduce the problem to a time-independent dc corona problem as before. Then they employed the numerical procedure developed earlier [13,14] to obtain the dc corona component in the ac conductors and the values of the ionic current density and electric field intensity at ground level.

Penner [4] has applied finite element method (FEM) to evaluate the ionic dc current injected from a dc line into an ac conductor during corona in a hybrid ac/dc transmission lines operating on a same tower. In his analysis, Deutsch's assumption was applied only on the artificial boundary and Kaptzov's assumption was used as the third boundary condition. The analysis is also based on the solutions to unipolar dc ionized field problem. A comparison of the calculated and experimental results for a laboratory line was presented in his studies along with the calculated data for a practical hybrid transmission line configuration.

2.3 CONCLUSIONS

In the solution methods of analyzing the ionized field problems of overhead transmission lines discussed above, the two fundamental assumptions usually employed by previous researchers are Deutsch's and Kaptzov's assumption. The validity of these assumptions has been repeatedly questioned in the literature [17-25]. Especially when Deutsch's assumption is employed, the distortion of the flux lines of dc transmission lines in corona is ignored, namely, the natural (equilibrium) relations among space charge, electric field intensity and space potential is destroyed.

The finite element method has been recognized as one of the most appropriate numerical techniques for the ionized field analysis because of both its generality and flexibility [17,21]. It does not rely on Deutsch's assumption. Therefore, a proposed computational algorithm that is based on the FEM will be discussed and implemented in the later chapters of this thesis.

Chapter 3
ITERATIVE FINITE ELEMENT PROCEDURE

This chapter introduces an iterative finite element procedure for the dc ionized field problem by using MANFEP [31]. First, the mathematical formulation has been done by employing Kaptzov's assumption as the third boundary condition and Deutsch's assumption on the artificial boundaries. Then by using triangular elements, the finite element (FE) procedure has been checked by applying it to a coaxial cylinder case. The different orders of polynomial approximations have also been compared in the procedure evaluation.

3.1 MATHEMATICAL FORMULATION FOR DC CORONA PROBLEM

3.1.1 Equations

Equations (2.1) - (2.4) can be combined in terms of Φ as follows:

$$\nabla \cdot (\nabla \Phi) = - \frac{\rho}{\varepsilon_o} \tag{3.1}$$

$$\nabla \cdot (k\rho \nabla \Phi) = 0 \tag{3.2}$$

Equations (3.1) and (3.2) are two coupled second order partial differential equations where the potential Φ and the charge density ρ are functions of the space coordinates. The simultaneous solutions of these two equations for Φ and ρ, being subject to proper boundary conditions, provides the solutions for the dc corona problem.

3.1.2 Boundary Conditions

As mentioned in Chapter 2, Equations (3.1) and (3.2) can be reduced to a nonlinear third order differential equation -- Equation (2.6). Thus, three boundary conditions are needed to determine the solutions for the boundary value problem.

The boundary conditions used in this method are as follows:

1. The potentials on the coronating dc conductors are known,

$$\Phi = V_{eq} \tag{3.3}$$

where V_{eq} is the equivalent dc potential to account for the ac potential in Geometry 1; $V_{eq} = V_{dc}$ in all the other geometries.

2. The potential on the non-coronating ac conductors and ground plane is known

$$\Phi = 0 \tag{3.4}$$

3. The electric field intensity on the coronating dc conductors is assumed constant at the onset value E_o, i. e.,

$$\left| \frac{d\Phi}{dn} \right| = E_o \tag{3.5}$$

where the value of E_o is determined by Peek's Law [28],

$$E_o = 30\, m \left(1 + \frac{0.301}{\sqrt{r_c}} \right) \quad (kV/cm) \tag{3.6}$$

in which r_c is the radius of the coronating conductor (in cm) and m is the surface factor which accounts for the degree of the roughness of the conductor. For Geometry 1, the surface factor is chosen to be 0.97 according to the ratio of the measured onset gradient and the one from Peek's Law when m = 1.0. For other full scale configurations (Geometries 2 to 5), fair weather conditions are assumed with m = 0.5 [3].

4. Appropriate space-charge-free field lines are taken as the artificial boundaries. This results in a natural Neumann boundary condition on these boundaries,

$$\frac{d\Phi}{dn} = 0 \tag{3.7}$$

However, when triangular elements with different densities are used to construct the mesh in the problem domain, as shown later on, the artificial boundary will be modelled by the straight sides of some of these triangles. The nodes of the big triangles, which are far away from the coronating conductor and used for modelling the farther part of the artificial boundary, will be displaced from the space-charge-free field line, and the boundary condition will not be the natural Neumann condition. Since this part of the boundary is far away from the coronating conductor, the space-charge-free potential is taken as the boundary condition,

$$\Phi = \Phi_{free} \tag{3.8}$$

3.2 OUTLINE OF ITERATIVE FINITE ELEMENT PROCEDURE

Since the exact distribution of the space charge density ρ in Equations (3.1) and (3.2) is not known initially, the algorithm begins with generating an approximated distribution for ρ. Then by solving Equations (3.1) and (3.2) iteratively, the final ρ

and the solutions of E and Φ would be reached with some tolerable errors. The following shows the logical iterative scheme using FEM:

1. Determine the problem domain.
2. Discretize the problem domain into triangular elements -- Mesh generation.
3. Specify initial values of ρ in the problem domain at all nodes.
4. Solve Equations (3.1) and (3.2) for the electric potential (Φ_1, Φ_2) and thus for the electric field intensity (E_1, E_2) in the problem domain by FEM, respectively. They will differ if the initiation of ρ is incorrect.
5. Update ρ at all nodes based on the differences between the solutions of Equations (3.1) and (3.2), i.e., between Φ_1 and Φ_2, E_1 and E_2, as well as the third boundary condition -- Equation (3.5)

6. Evaluate the differences of the solutions from Equations (3.1) and (3.2); then repeat steps 4 - 6 until the following convergence criteria are satisfied simultaneously,

$$|\Phi_1 - \Phi_2| \leq \delta_1 \Phi_{av}$$

$$|\rho_{new} - \rho_{old}| \leq \delta_2 \rho_{old}$$

$$|E_1 - E_2| \leq \delta_3 E_{av}$$

$$|E_{c1} - E_{c2}| \leq \delta_4 E_o$$

where ρ_{new} and ρ_{old} are the new and the old approximations for the space charge density; E_{c1} and E_{c2} are the magnitudes of the electric field intensity at the conductor solved from Equations (3.1) and (3.2), respectively; δ_1, δ_2, δ_3 and δ_4 are small deviations specified according to the desired accuracy. In this work the values assigned to δ_1, δ_2, δ_3 and δ_4 were 0.01, 0.01, 0.01, and 0.05, respectively; Φ_{av} and E_{av} are the average value of Φ_1 and Φ_2, and of E_1 and E_2 respectively.

7. Determine the field quantities (E, ρ, J) at ground level from the final solutions for the ionized field.

Based on the above steps, by using MANFEP in step 4, an iterative finite element program has been written. An automatic mesh generation program has first been developed.

3.3 DETERMINATION OF THE PROBLEM DOMAIN

It is well-known that FEM has to be applied to bounded regions where the solutions are required. One effective and simple way to determine the problem domains is to trace the space-charge-free field lines leaving the coronating dc conductors [4]. Generally, in a hybrid ac/dc line geometry as shown in Fig. 1.2, the problem domain can be divided into the following regions by assuming ac conductors at zero potential:

- Between positive and negative dc conductors;
- Between positive (negative) dc conductor and each of the three phase ac conductors;
- Between positive (negative) dc conductor and ground.

The last region is the problem domain in which the solutions will be discussed in this thesis since the aim of the work is to calculate E, ρ, and J at ground level.

3.3.1 Determination of the Space-Charge-Free Field

The space-charge-free field is the electric field determined without considering the effect of corona-generated space charges. Since the ratios H/r (height / radius) for all the line geometries in this thesis are greater than ten, the Method of Images can be used to determine the space-charge-free field. Assuming that each conductor can be approximated by an infinite line of charge located at the center of the conductor, the magnitude of the charges for each lines is obtained from the following set of simultaneous equations:

$$V_i = \frac{1}{2\pi \varepsilon_o} \sum_{j=1}^{N} Q_j \ln \frac{D^-_{ij}}{D^+_{ij}}, \qquad i = 1, ..., N \tag{3.9}$$

where V_i is the potential on the conductor i; D^-_{ij} represents the distance from the i^{th} conductor to the image of the j^{th} line charge; D^+_{ij} is the distance between the i^{th} and j^{th} conductors; N is the set of all conductors without including the imaged ones.

Knowing the charges Q_j on each conductor, the space-charge-free potential and field intensity at any point P in the problem domain can be determined as follows:

$$\Phi_p = \frac{1}{2\pi\,\varepsilon_o} \sum_{j=1}^{N} Q_j \ln \frac{D^-_{pj}}{D^+_{pj}} \tag{3.10}$$

and

$$\mathbf{E}_p = \frac{1}{2\pi\,\varepsilon_o} \sum_{j=1}^{N'} Q_j \frac{\mathbf{d}_{jp}}{|d_{jp}|^2} \tag{3.11}$$

where $\mathbf{d}_{jp}$ is the distance vector from the line of charge j to the point P, N' is the set of all conductors including the imaged ones.

The derived formula for the space-charge-free fields of the line geometries are given in Appendix A.

3.3.2 Determination of the Problem Domain

The drift of ions generated by corona on the dc line conductors is described by the following equation:

$$\mathbf{V} = \frac{d\mathbf{r}}{dt} = k\,\mathbf{E}\,(\mathbf{r}, t) \tag{3.12}$$

where **E** is the space-charge-free field intensity at any point in space, **V** is the velocity of the ion at that point, **r** is the position vector, and k is the mobility of the ions.

Equation (3.12) can be separated into the following two scalar equations:

$$v_x = \frac{dx}{dt} = k\, E_x\,(x, y, t) \tag{3.13}$$

$$v_y = \frac{dy}{dt} = k\, E_y\,(x, y, t) \tag{3.14}$$

The trajectories of ions can be determined by integrating the above equations numerically with respect to time t using the Runge-Kutta method [29].

Figures 3.1 - 3.5 show the ion trajectories of the boundaries for the different regions, where θ is the angle of the dc conductor node on the dc conductor where the field line originates. θ=0 corresponds to the lowest point on the dc conductor. Due to the symmetry, only half of the line geometry is considered. The shaded regions are the problem domain of interest. Since the space-charge-free field lines are taken as the artificial boundaries, Deustch's assumption is resorted on the boundaries only.

In Figure 3.1, Line 2 is next to the field line on the ac conductor (Line 1). The flux line that intersects the ground plane far enough from the origin has been chosen as Line 3, to ensure that the ionized field at the intersection point is very small. In this

way, the shaded problem domain covers the region of interest, i.e., the area where the field quantities at ground (E, ρ, J) is to be determined. Similarly, in Figure 3.2, Figure 3.3, and Figure 3.5, Line 2 is right next to the field line terminated at -dc conductor (Line 1) as one part of the artificial boundary, while Line 3 has been chosen in the same way as in Figure 3.1 as the other part of the artificial boundary. In Figure 3.4, however, Line 2 is right next to the field line terminated at the ac (phase C) conductor (Line 1). In Figure 3.2 to 3.5, Line 4 is part of the flux line terminated at -dc conductor. From the θ values of Line 2 in these figures, it can be seen that even for space-charge-free electric field, the shielding effect of the ac conductors is different with the different arrangement of the conductors, i.e., with the bigger shielding effect in Geometry 4 compared with the ones in Geometries 2 and 3. In the laboratory line (Geometry 1), it has been found out that the shaded region in Figure 3.1 is approximately irrespective of the ac applied voltages[4]. Therefore, this region can also be used as the problem domain when the ac voltage is not zero.

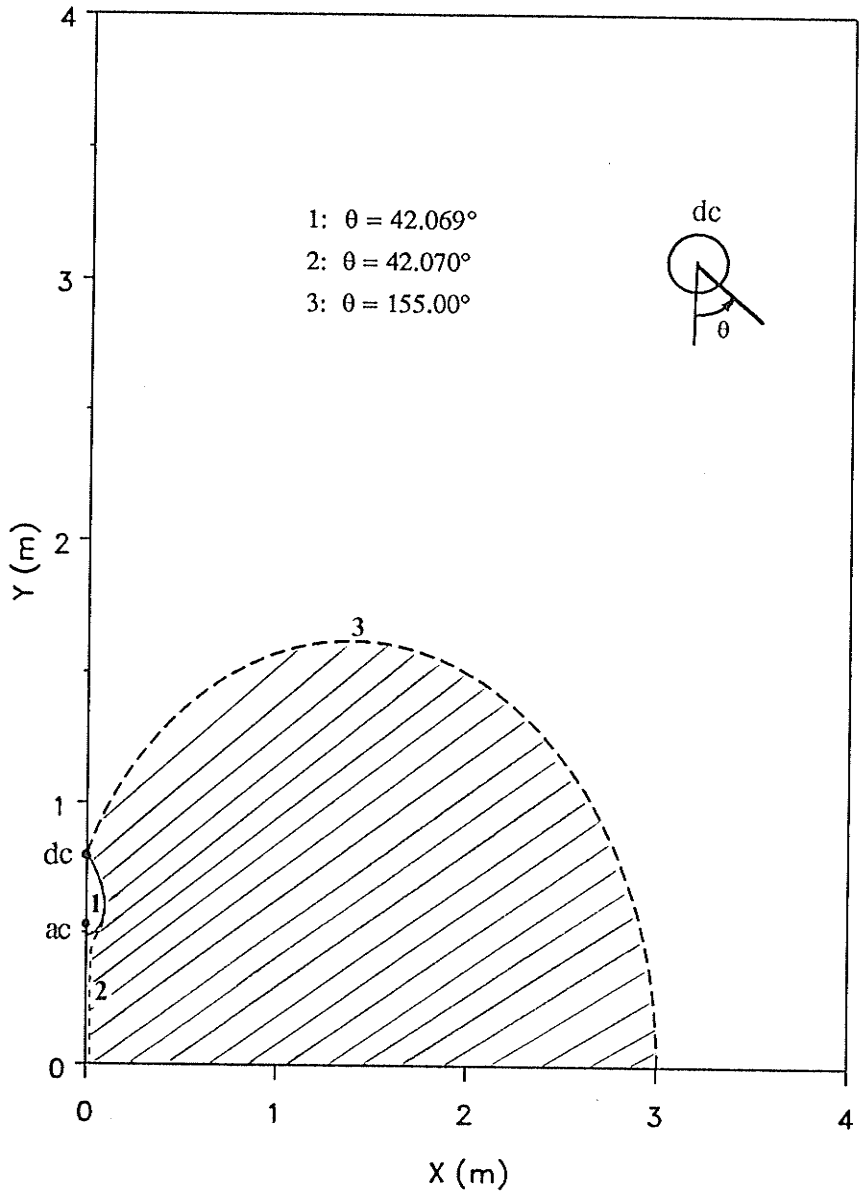

Figure 3.1: *Ion Trajectories in the Laboratory Line System (Geometry 1),* V_{ac}*=0,* V_{dc}*=60kV*

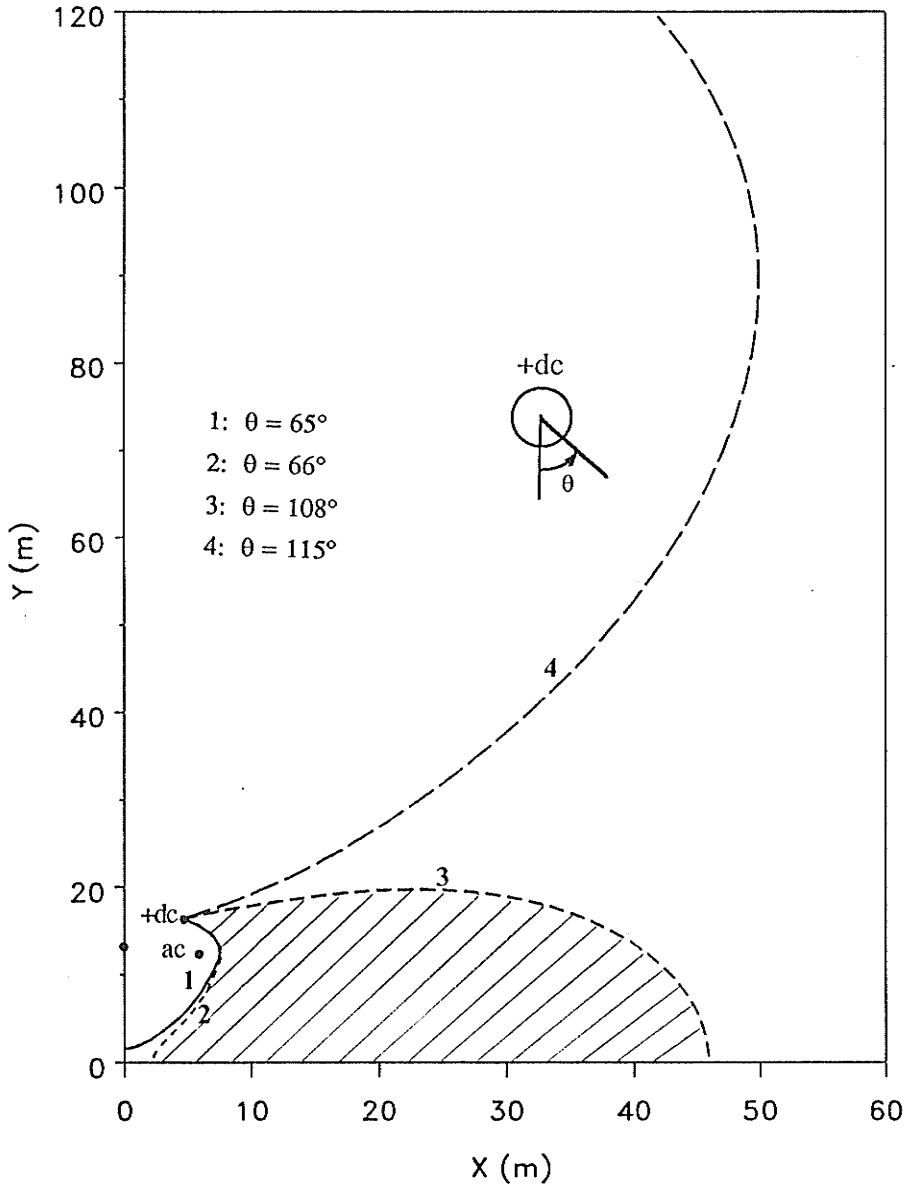

Figure 3.2: *Ion Trajectories in Geometry 2 System, V_{ac}=0, V_{dc} = 300 kV*

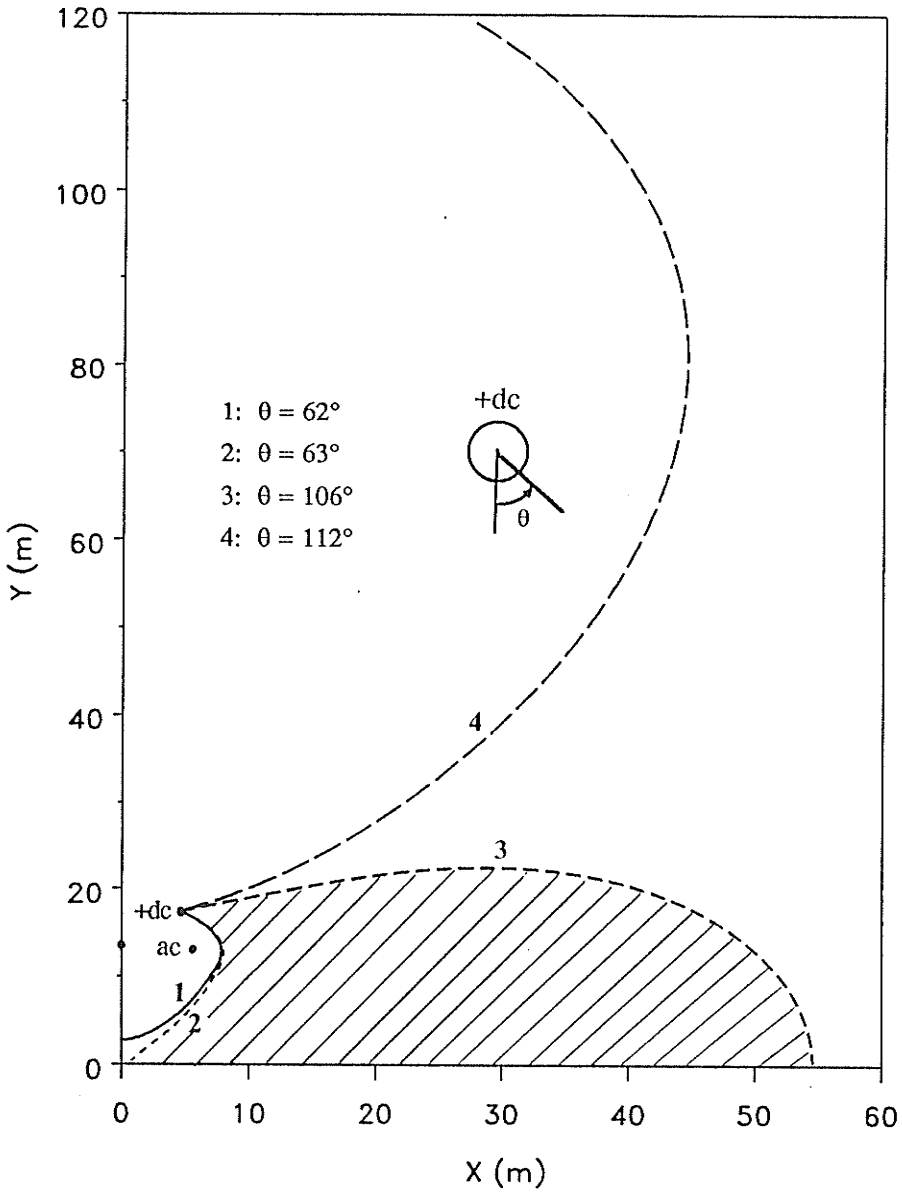

Figure 3.3: *Ion Trajectories in Geometry 3 System, V_{ac}=0, V_{dc} = 300 kV*

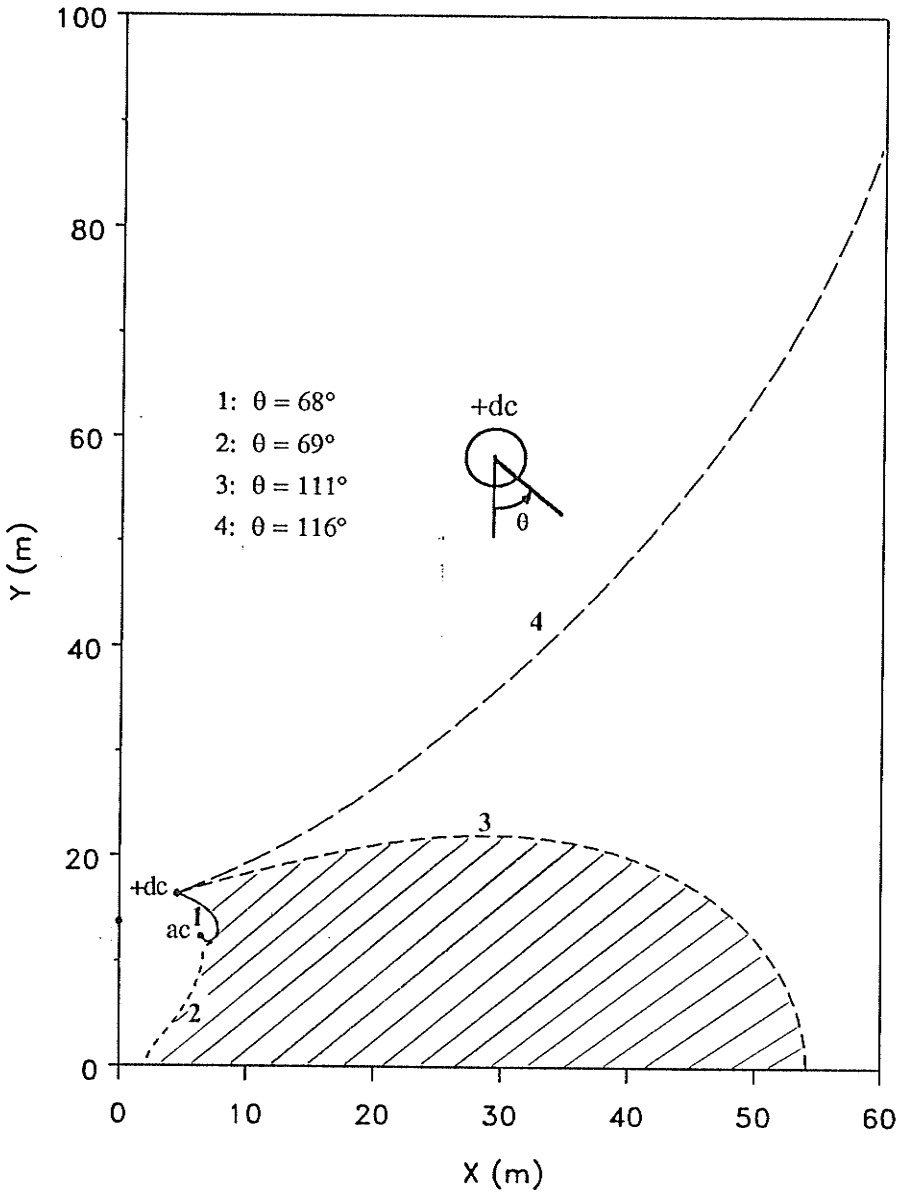

Figure 3.4: *Ion Trajectories in Geometry 4 System, V_{ac}=0, V_{dc} = 300 kV*

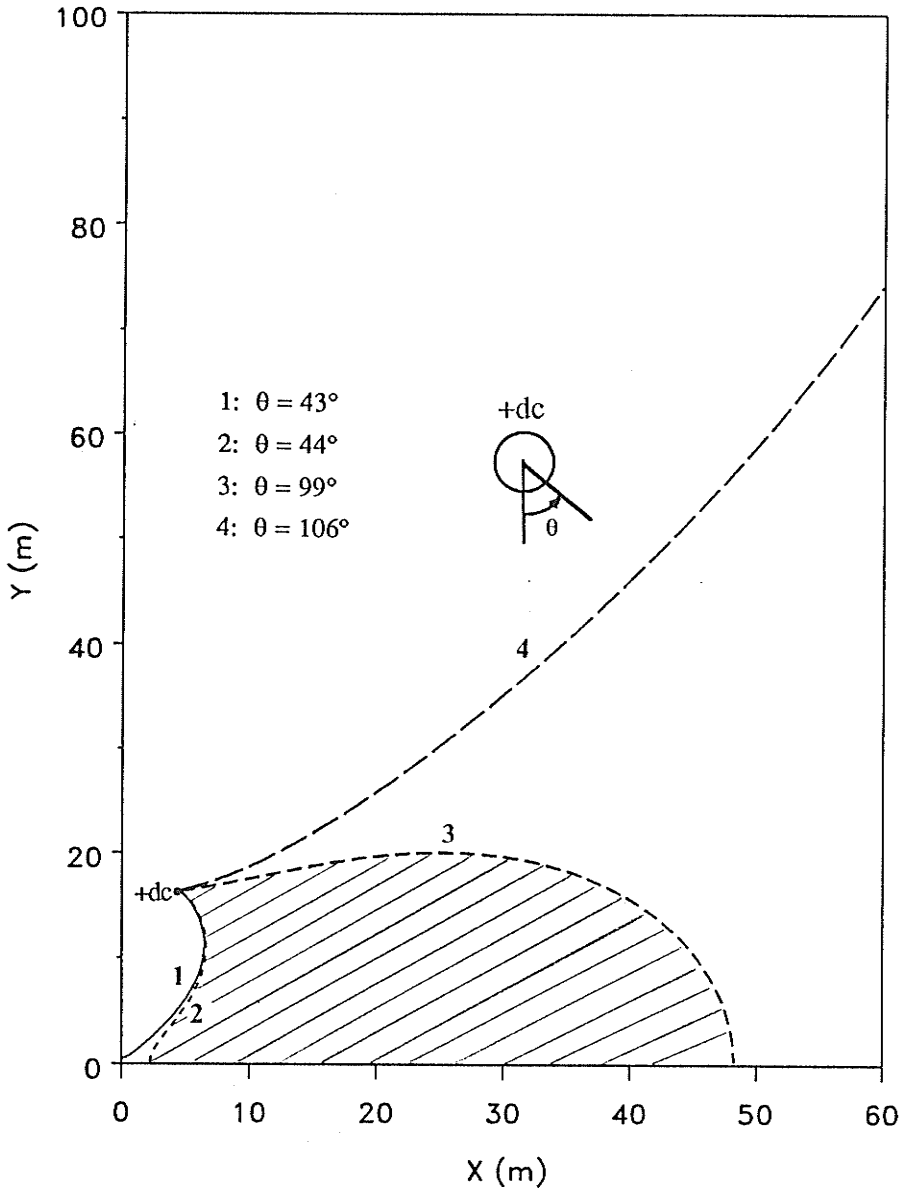

Figure 3.5: *Ion Trajectories in Geometry 5 System, V_{dc} = 300 kV*

3.4 MESH GENERATION PROCEDURE

Triangular elements are used in the iterative finite element program. In order to reduce the tedious work in formulating the triangle mesh, an automatic mesh generation program has been developed. Initially, a number of nodes (triangle vertices) are chosen evenly on the conductor surface. Starting from one conductor node, the second node is placed on the field line by a distance $L_o=r_c(\Delta\theta)$ from the conductor node, where $\Delta\theta$ is the angle subtended at the conductor center by a chord joining two consecutive conductor nodes, and r_c is the conductor radius. Each segment, moving away from the conductor, increases in length by a weighting factor, WF.

$$\text{Length of segment } i = (WF)^{i-1} (r_c \Delta\theta)$$

where i = 1 corresponds to the first node away from the conductor and is increased by 1 for the subsequent nodes.

The input data to the program consists of the total number of the conductor nodes (N_{dc}), the radius of the conductor (r_c), and the weighting factor (WF). The output consists of firstly the x and y coordinates of each point with its corresponding number, and secondly the element number with its element definition in the counter-clockwise direction in order to match with MANFEP. Both nodal numbers and element numbers are arranged in sequential order.

By using the mesh generation program, the triangular meshes for Geometries 1 to 5 are generated and shown in Figures 3.6 - 3.10, where IN represents the number of

the initial nodes or triangle vertices; NT is the total number of the elements.

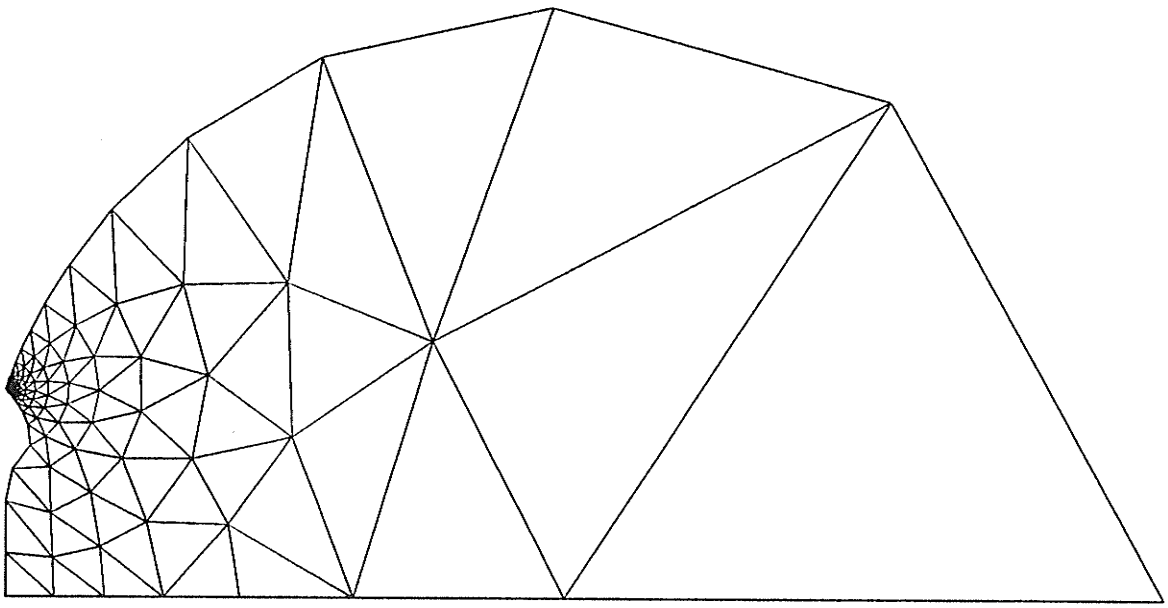

Figure 3.6: *Finite Element Mesh for Geometry 1, IN = 160, NT = 264*

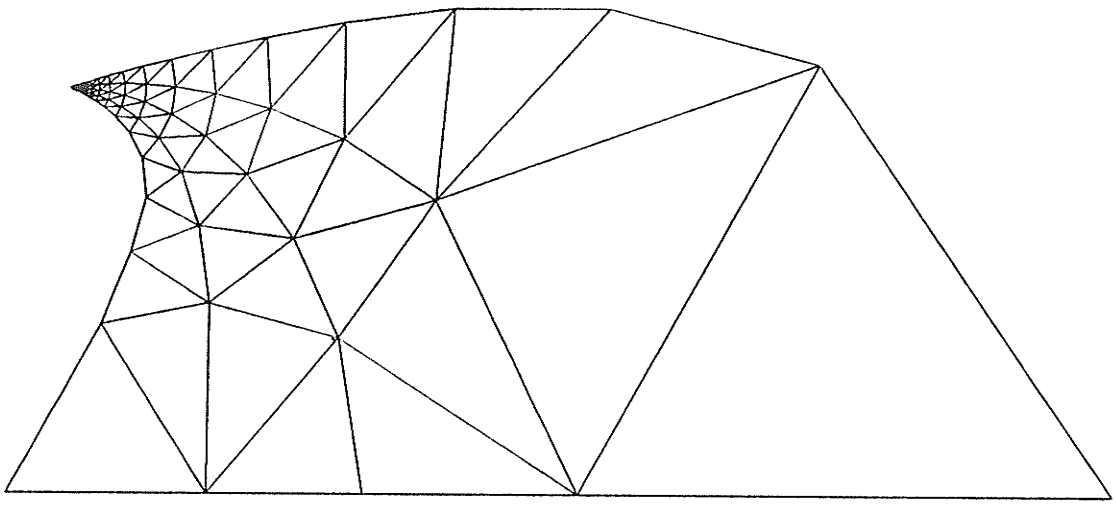

Figure 3.7: *Finite Element Mesh for Geometry 2, IN = 115, NT = 175*

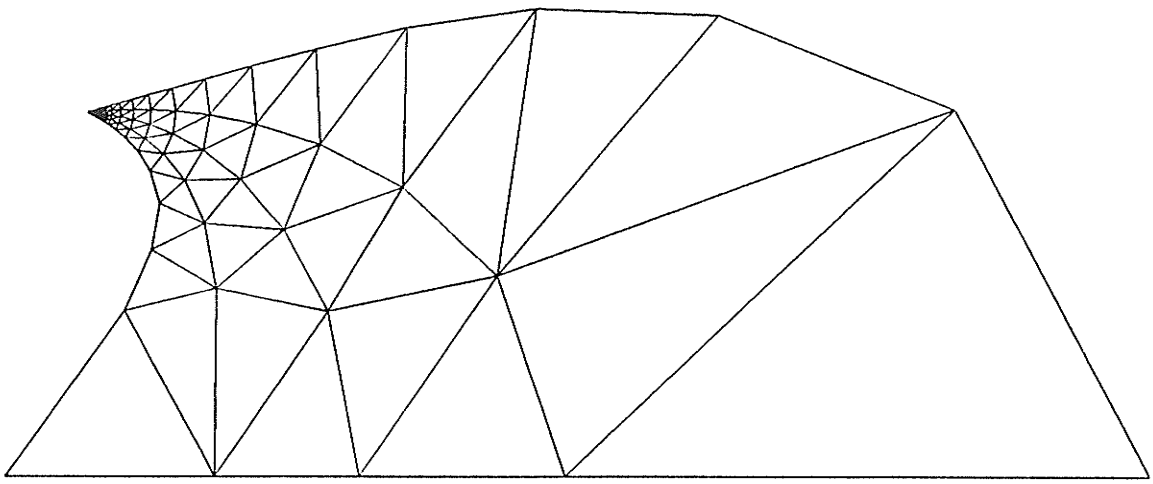

Figure 3.8: *Finite Element Mesh for Geometry 3, IN = 117, NT = 178*

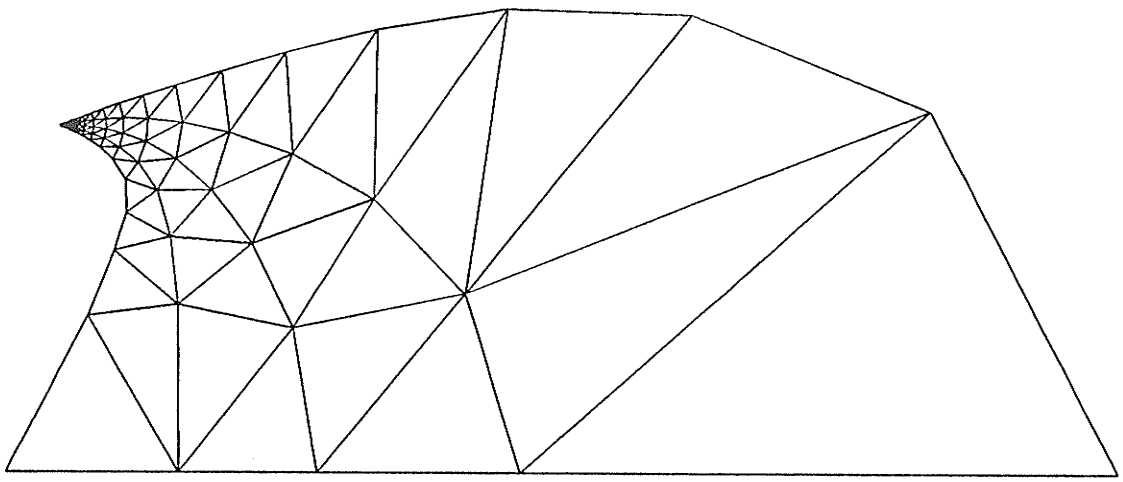

Figure 3.9: *Finite Element Mesh for Geometry 4, IN = 117, NT = 178*

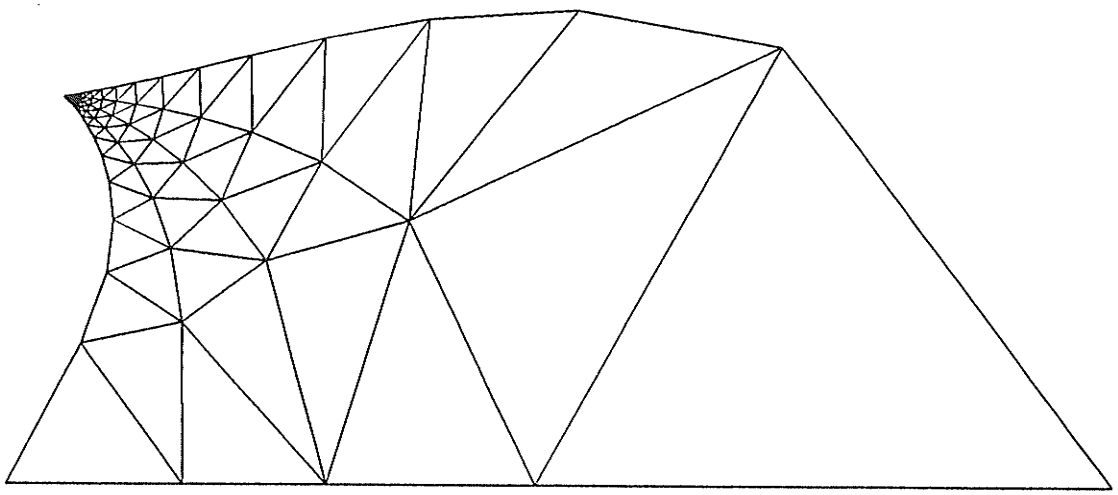

Figure 3.10: *Finite Element Mesh for Geometry 5, IN = 114, NT =173*

3.5 APPLICATION TO COAXIAL CYLINDER GEOMETRY

Since the unipolar dc corona problem described by Equation (2.6) can only be solved analytically for a simple case of coaxial cylinder geometry, the numerical algorithm of FE procedure presented above can be checked by applying it to such a case and comparing the numerical results with the exact ones.

3.5.1 Geometry and Mesh Generation

Chosen from reference [21], the coaxial cylindrical conductor is shown in Figure 3.11.

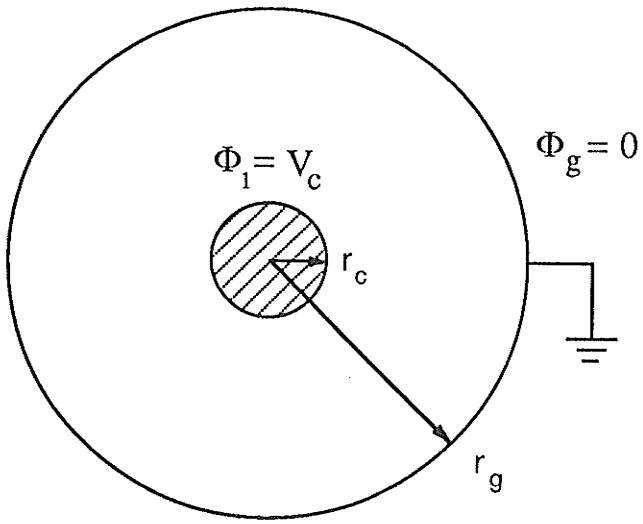

Figure 3.11: *Coaxial Cylindrical Configuration*

where $r_c = 0.1$ cm, $r_g = 2.0$ cm. From Peek's Law, the onset field intensity E_o is equal to 58.56 kV/ cm, which corresponds the onset voltage V_o to 17.542 kV. The applied voltage on the inner conductor V_c is 1.42Vo, i.e., $V_c = 24.909$ kV.

Due to symmetry of the problem, only a quarter of the geometry is considered.

Figures 3.12 and 3.13 show the problem domain and the finite element mesh.

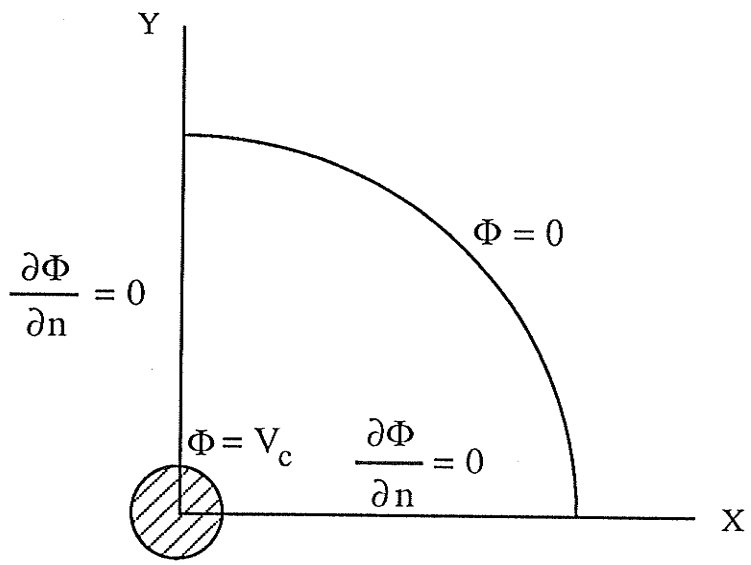

Figure 3.12: *Problem Domain for the Coaxial Cylinder Geometry*

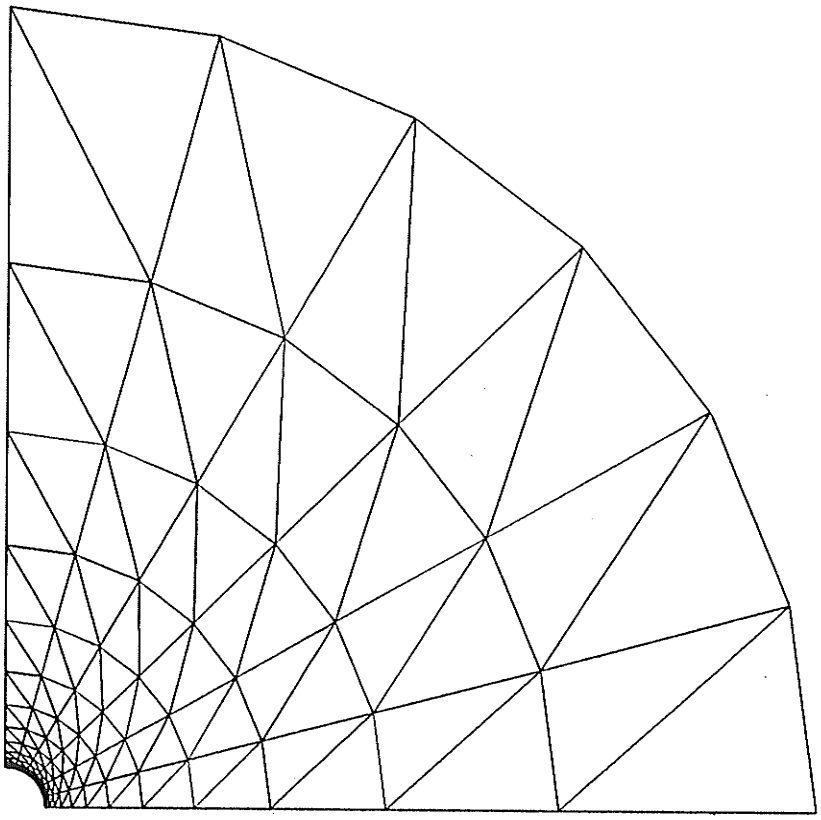

Figure 3.13: *Finite Element Mesh for the Coaxial Cylinder Geometry, IN =98, NT = 156*

3.5.2 Evaluation of the FE Procedure

The initial space charge density ρ has been chosen by using the closed-form (A.2.3) from the Appendix A. Then the solutions by FEM of Equation (3.1) should not differ much from the ones of Equation (3.2) since ρ is close to the real charge distribution.

Table 3.1 shows the errors after solving the Equations (3.1) and (3.2) at the centroid of each element only once. (i. e., one iteration)

Table 3.1: *Errors in the Evaluation of the FE Procedure*

NDEG	δE (%)	δV (%)	δρ (%)	EDIFF (%)	VDIFF (%)	RDIFF (%)	CPU (sec)
2	1.67	2.26	0.0	1.80	4.63	1.25	45
3	1.66	2.23	0.0	1.80	4.41	1.25	106

where

$$\delta E = \left[\frac{E_{1i} - E_{2i}}{E_{avi}}\right]_{RMS} = \sqrt{\frac{\sum_{i=1}^{NT}\left[\frac{(E_{1i} - E_{2i})}{(E_{1i} + E_{2i})/2}\right]^2}{NT}} ,$$

$$\delta V = \left[\frac{\Phi_{1i} - \Phi_{2i}}{\Phi_{avi}}\right]_{RMS} , \qquad \delta \rho = \left[\frac{\rho_{new\,i} - \rho_{old\,i}}{\rho_{old\,i}}\right]_{RMS} ,$$

$$EDIFF = \left[\frac{E_{ex\,i} - E_{av\,i}}{E_{ex\,i}}\right]_{RMS} , \qquad VDIFF = \left[\frac{\Phi_{ex\,i} - \Phi_{av\,i}}{\Phi_{ex\,i}}\right]_{RMS} ,$$

$$\text{RDIFF} = \left[\frac{\rho_{ex\,i} - \rho_i}{\rho_{ex\,i}} \right]_{\text{RMS}} ,$$

where, RMS represents the root mean square value and the difference is determined over all the triangle centroids.

E_{1i} , E_{2i} : the magnitudes of the electric field intensity at the centroid of element i, determined from Equations (3.1) and (3.2), respectively.

Φ_{1i} , Φ_{2i} : the potentials at the centroid of element i from Equations (3.1) and (3.2), respectively.

E_{avi} , Φ_{avi} : the average values of E_{1i} and $E_{2\,i}$, $\Phi_{1\,i}$ and $\Phi_{2\,i}$, respectively.

$\rho_{new\,i}$, $\rho_{old\,i}$: the new and the old approximations for the space charge density of element i at the centroids, respectively.

E_{exi} , Φ_{exi} , ρ_{exi} : the exact solutions from the equations (A.2.2), (A.2.1), and (A.2.3) from the Appendix A, respectively.

ρ_i : the numerical approximations for the space charge density of element i.

NDEG is the degree of the approximating polynomials which refers to the order of

polynomial approximation for the potential within an element. The higher the value of NDEG is, the more accurate the solutions will be. However, the computer storage and CPU time will also increase tremendously. In Table 3.1, second and third order polynomials were used.

From the results, it can be seen that the program is functioning properly. When the initial charge distribution is close to the exact one, the solutions of Equation (3.1) are very close to the ones of Equation (3.2). The relative errors of the electric field intensity and the potential are only 1.7% and 2.3%, respectively. Moreover, the calculated values are also very close to the exact ones, the relative errors of the electric field and potential are within 5%.

Another conclusion is that the second-order isoparametric triangular elements with curved elements on the coronating conductor surface provides satisfactory results and saves a lot of computer time compared with the cubic polynomial approximation as shown in Table 3.1. Therefore, the quadratic polynomials are used to describe the potential variation within each element throughout this thesis.

Chapter 4
APPLICATION TO HYBRID AC/DC LINES

This chapter details the solutions for the ionized field of the hybrid line Geometries 1 to 4 using the iterative finite element procedure discussed in Chapter 3. For the purpose of analyzing the shielding effect of the ac conductors in the hybrid lines, one bipolar line geometry (Geometry 5) has also been studied.

4.1 MESH GENERATION AND EVALUATION

Following the mesh generation procedure developed in Section 3.4, different meshes were constructed and evaluated. The formulation of a mesh has a significant effect on the accuracy of FE solutions [4]. The meshes can be evaluated by comparing the solutions for the space-charge-free electric field determined by FEM with the ones obtained by the method of images described in Subsection 3.3.1.

Tables 4.1 & 4.2 show the errors corresponding to various finite element meshes, where

- N_{dc} - number of nodes on the dc conductor.

- L_o - initial segment length from dc conductor.
- r_{dc} - radius of the dc conductor.
- WF - weighting factor.
- IN - initial nodes (triangle vertices) in a mesh.
- NT - number of triangular elements in a mesh.
- Nodal Error, Centroid Error, DC Cond. Error, Ground Nodal Error - the relative differences between the numerical (Finite Element) and analytical (image method) solutions for the potential and the magnitude of the electric field intensity at all nodes, the triangle centroids, the conductor nodes, and the ground nodes, respectively.
- RMS - root mean square.
- Max. - maximum nodal error.

Table 4.1: *Errors for Various Meshes, Geometry 1, $V_{ac} = 0$, $V_{dc} = 60$ kV*

Mesh		1D1A1	1D1A2	1D1A3	1D1A4	1D1A5	1D1A6
N_{dc}		9	9	9	8	9	9
L_o		r_{dc}	$0.3\, r_{dc}$	$0.5\, r_{dc}$	$0.5\, r_{dc}$	$0.3\, r_{dc}$	$0.3\, r_{dc}$
WF		1.5	1.5	1.5	1.5	1.6	1.4
IN		162	189	180	160	170	221
NT		270	318	302	264	285	375
V Nodal Error (%)	RMS	0.46	0.46	0.65	0.69	0.46	0.48
	Max.	3.84	4.44	7.30	7.75	3.14	5.51
V Centroid Error (%)	RMS	1.09	0.99	0.90	0.78	1.08	0.77
	Max.	12.16	11.97	10.52	8.78	13.54	10.9
E Nodal Error (%)	RMS	5.96	3.63	4.08	3.83	4.0	3.15
	Max.	21.8	21.2	17.03	16.57	16.3	25.8
E Centroid Error (%)	RMS	1.43	1.09	1.31	1.31	1.18	0.88
	Max.	9.09	10.15	15.1	15.1	7.10	13.4
E DC cond.nodal Error, RMS (%)		10.8	1.51	3.25	6.49	1.55	1.34
E Ground Nodal Error, RMS (%)		11.6	11.3	9.24	6.90	8.53	6.68

Table 4.2: *Errors for Various Meshes, Geometry 2 & 3, V_{ac}= 0,V_{dc} =± 300 kV*

Geometry 2								Geom. 3
Mesh		2D3A1	2D3A2	2D3A3	2D3A4	2D3A5	2D3A6	3D3A
N_{dc}		5	5	5	4	5	5	5
L_o		r_{dc}	$0.3\,r_{dc}$	$0.5\,r_{dc}$	$0.5\,r_{dc}$	$0.3\,r_{dc}$	$0.3\,r_{dc}$	$0.3\,r_{dc}$
WF		1.5	1.5	1.5	1.5	1.6	1.4	1.4
IN		84	99	93	75	88	115	117
NT		125	149	140	106	132	175	178
V Nodal Error (%)	RMS	0.48	0.46	0.54	0.51	0.58	0.33	0.44
	Max.	1.38	1.30	2.30	2.63	1.80	1.28	1.84
V Centroid Error (%)	RMS	1.09	0.99	1.59	1.19	1.11	0.83	1.04
	Max.	7.00	6.91	12.9	10.66	6.73	7.22	8.5
E Nodal Error (%)	RMS	5.09	3.4	3.97	4.25	4.60	2.79	5.76
	Max.	14.5	14.2	13.1	20.1	16.9	12.8	17.7
E Centroid Error (%)	RMS	1.39	0.99	0.99	0.95	1.27	0.63	0.77
	Max.	4.06	3.90	3.45	2.44	4.39	2.95	4.38
E DC cond.nodal Error, RMS (%)		8.89	2.15	5.68	5.32	2.05	2.25	2.20
E Ground Nodal Error, RMS (%)		8.45	8.26	7.73	11.94	9.40	8.72	4.87

The above two tables show that the FE procedure is more accurate at centroids than at nodes as concluded in [4]. The maximum errors (Max.) occur at nodes on the artificial boundary and at the centroids of triangles adjacent to the artificial boundary. The FE procedure gives less accurate results near the artificial boundaries. The accuracy of the electric field around the conductor surface increases as the number of conductor nodes increase and the density of the triangles around the conductor increases (L_o decreases). In general, an increase in the number of triangular elements (NT) improves the accuracy of a mesh but also increases the CPU time.

All the meshes in Tables 4.1 & 4.2 use second order elements. Mesh 1D1A6 is chosen for the FE solution for Geometry 1. Meshes 2D3A6 and 3D3A are chosen for Geometries 2 and 3, respectively. For Geometries 4 and 5, the same N_{dc}, L_o, and WF are used as in Mesh 2D3A6.

4.2 INITIAL APPROXIMATION FOR THE SPACE CHARGE DENSITY

The initial distribution of the charge density ρ at the finite element nodes is obtained by employing an equivalent coaxial cylindrical system with the inner radius equal to the radius of the coronating dc conductor (r_c) and outer radius R determined by :

$$R = r_c \exp\left(\frac{V_{dc}}{E_{max}\, r_c}\right) \tag{4.1}$$

where E_{max} is the maximum space-charge-free electric field on the surface of the dc

conductor in the actual geometry and V_{dc} is the potential of the dc conductor in the actual geometry.

Therefore, the space charge density on the inner conductor in the equivalent concentric cylinder system ρ_0 can be obtained by the implicit equation (A.2.4), from the Appendix A.

Assuming that the maximum space charge on the dc conductor surface for the actual line is equal to ρ_0 and the space charge distribution on the dc conductor is to vary in the following form:

$$\rho_c (\theta) = 0.5\, \rho_0 \,(1+ \cos\theta) \tag{4.2}$$

where θ is the angle of the dc conductor node on the dc conductor where the field line originates, and θ equals zero corresponding to the maximum space-charge-free field on the dc conductor surface.

The space charge density at any point along a space-charge-free electric field line is given by the known analytical solution for the coaxial cylinder geometry [21],

$$\rho\ (\theta, r) = \frac{\sqrt{r_c\, E_o\, \varepsilon_o\, \rho_c(\theta)}}{\sqrt{L^2 + K_2^2 - r_c^2}} \tag{4.3}$$

where

$$K_2 = \sqrt{\frac{r_c\, E_o\, \varepsilon_o}{\rho_c\, (\theta)}}\ ,$$

and L is the length of the field line from the dc conductor node to the point of interest in the problem domain.

4.3 UPDATE ALGORITHMS

As mentioned in Section 3.2, the update algorithm is based on the approximation for the space charge ρ and the simultaneous solutions of Equations (3.1) and (3.2), along with the third boundary condition (Kaptzov's assumption). In general, an update algorithm has the following form,

$$\rho_{new} = \rho_{old}\, f\,(\Delta\Phi, \Delta E, \Delta E_c) \tag{4.4}$$

where ρ_{new} is the updated charge density at the node and ρ_{old} is the charge density at the same node used in the previous iteration; $\Delta\Phi=\Phi_1-\Phi_2$, $\Delta E=E_1- E_2$, $\Delta E_c=E_{c1}- E_{c2}$ are the discrepancies between the solutions from Equations (3.1) and (3.2) for the potential, field intensity and the field intensity on the dc conductor surface, respectively. The function $f\,(\Delta\Phi, \Delta E, \Delta E_c)$ should be 1 when convergence occurs.

Different approaches have been employed in the literature. Abdel-Salam et al. [18] used an updating formula based on the differences between Φ_1 and Φ_2 only. No information was given on the enforcement of the third boundary condition. Gela [30] used a correction formula based only on the deviations of E_{c1} and E_{c2} from the Kaptzov's boundary condition. In the present work, two different update algorithms have been examined for the different line geometries.

4.3.1 Update Algorithm for Geometry 1

The following equation was used in the update algorithm for Geometry 1,

$$\rho_{newi} = \rho_{oldi} \left[\frac{0.5\ (E_{1j}+E_{2j})}{E_o} \right]^{a} \left[1 + \alpha \frac{E_{1i}-E_{2i}}{E_{1i}+E_{2i}} \right] \left[1 + \gamma \frac{\Phi_{1i}-\Phi_{2i}}{\Phi_{1i}+\Phi_{2i}} \right] \qquad (4.5)$$

where a, α, and γ are parameters chosen to ensure convergence. Different choices of these parameters affect the speed of convergence significantly as shown in Table 4.3. δE, δV, and $\delta\rho$ in Table 4.3 are the RMS errors at the triangle centroids which have the same expressions as given in Subsection 3.5.2; δE_{c1} and δE_{c2} are defined as:

$$\delta E_{c1} = \left[\frac{E_o - E_{1j}}{E_o} \right]_{RMS} \quad \text{and} \quad \delta E_{c2} = \left[\frac{E_o - E_{2j}}{E_o} \right]_{RMS},$$

where E_{1j} and E_{2j} are the magnitudes of the electric field intensity at dc conductor node j obtained from equations (3.1) and (3.2), respectively; the RMS error is computed over the dc conductor nodes.

The last column in Table 4.3 gives the number of iterations.

Table 4.3: *Convergence for Different Constants a, α, and γ, Geometry 1,* $V_{ac} = 0$, $V_{dc} = 60\ kV$

a	α	γ	δE (%)	δV (%)	δρ (%)	δE_{c1} (%)	δE_{c2} (%)	Iter. #
-0.1	-2.4	0.0	0.83	0.91	0.96	4.5	4.0	5
0.5	-2.4	0.0	0.81	0.99	2.4	3.6	3.0	4
1.0	-2.4	0.0	0.80	0.89	2.8	3.0	2.5	4
-0.1	-2.4	-1.0	0.93	0.74	1.0	4.5	3.0	4
-0.1	-2.4	-1.5	Diverge					
-0.1	-1.0	-1.0	0.80	0.76	0.82	4.9	3.3	10
-0.1	-2.0	-1.0	0.78	0.87	0.87	4.6	3.1	5
0.5	-2.4	-1.0	0.72	1.0	2.2	3.0	3.6	5
-0.1	-3.0	-1.0	Diverge					
1.2	-2.4	0.0	0.79	0.86	2.8	1.8	3.0	4
-0.5	-2.4	0.0	Diverge					
-0.1	-2.2	-1.0	0.96	0.77	1.0	4.4	3.0	4
1.0	-2.4	0.5	0.88	1.0	2.5	1.8	3.1	6
-0.1	-1.5	-1.0	0.90	0.80	0.81	4.9	4.6	6
1.5	-2.4	-1.0	0.84	1.0	4.0	2.1	2.0	19

Figure 4.1(a) - Figure 4.2 show the convergence of the iterative procedure, i.e., the changes in δV, δE, $\delta \rho$, δE_{c_1}, and δE_{c_2} with respect to the number of iterations for a=-0.1, α=-1.0, and γ=-1.0. Figure 4.1(a) - Figure 4.1(c) also compare the convergence of the iterative procedure with two different initial space charge distributions. The solid curve represents the results with an initial charge distribution given by Equation (4.3) and the dashed curve with an initial charge distribution obtained by increasing the first one by 50%. It can been seen that in spite of the significant initial errors, the algorithm works its way through to convergence.

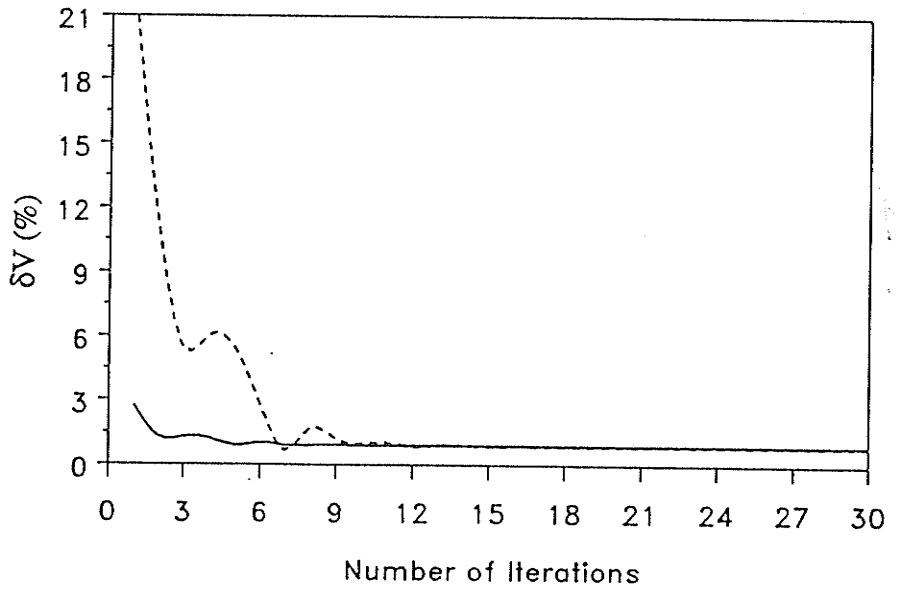

Figure 4.1(a): *Deviation δV vs Number of Iterations*

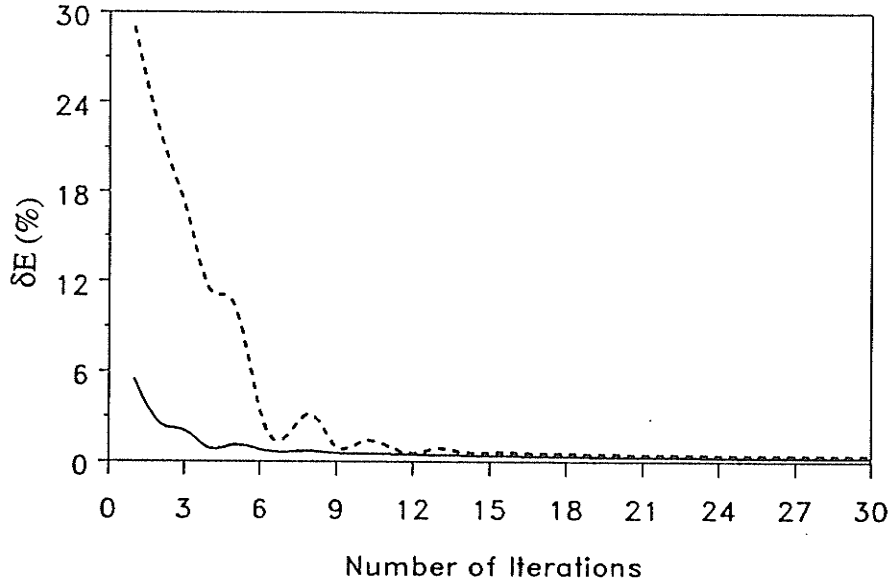

Figure 4.1(b): *Deviation δE vs Number of Iterations*

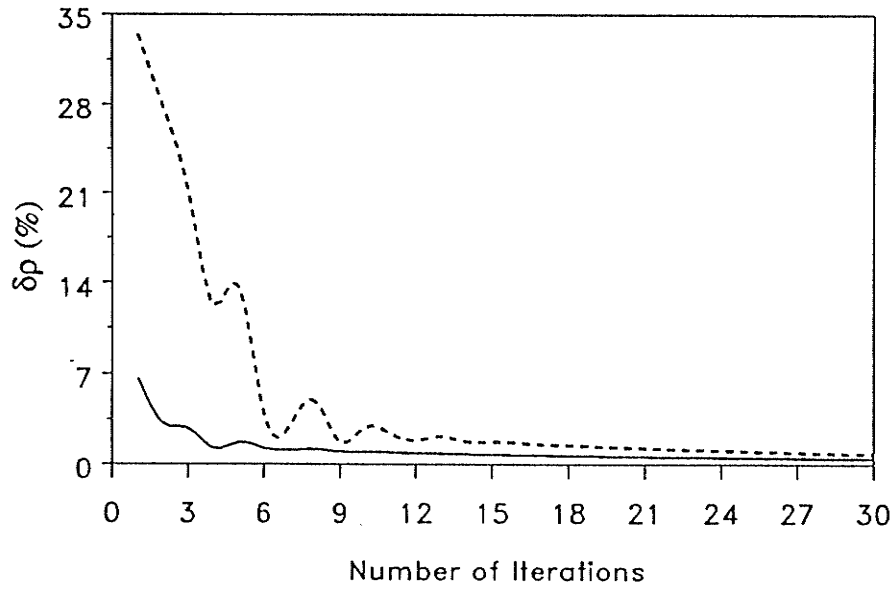

Figure 4.1(c): *Deviation δρ vs Number of Iterations*

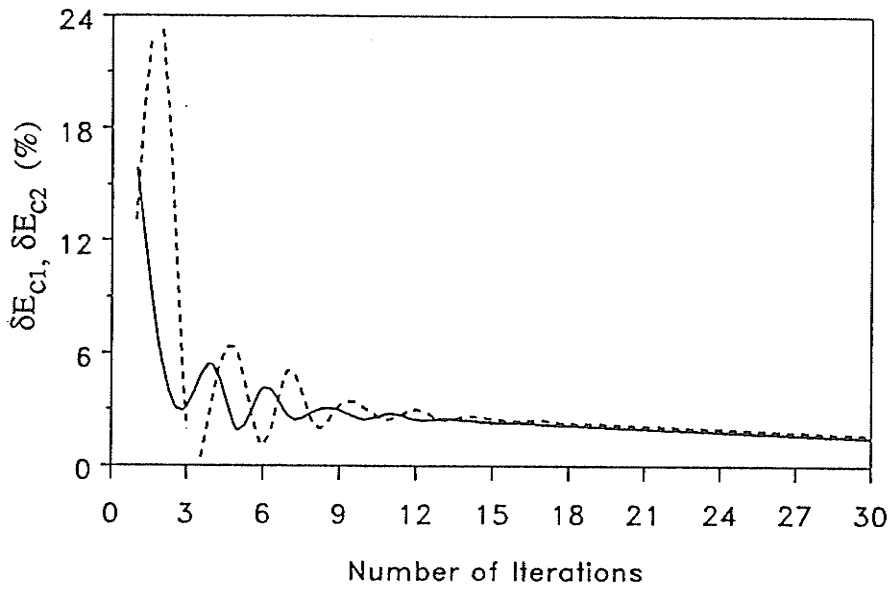

Figure 4.2: *Deviations δE_{c1} and δE_{c2} vs Number of Iterations*

4.3.2 Update Algorithm for Geometries 2 to 5

When Equation (4.5) is applied to Geometries 2 to 5, the parameters a, α, and γ cannot be easily found to ensure convergence. Since the update algorithm is not unique for a certain geometry, the following equation is used for updating the space charge density for Geometries 2 to 5,

$$\rho_{newi} = \rho_{oldi}\left[1+\alpha\frac{E_{1i}-E_{2i}}{E_{1i}+E_{2i}}\right]^{b}\left[1+\gamma\frac{\Phi_{1i}-\Phi_{2i}}{\Phi_{1i}+\Phi_{2i}}\right]\left\{\left[1+\beta\frac{E_o-E_{1j}}{E_o}\right]\left[1+\eta\frac{E_o-E_{2j}}{E_o}\right]\right\}^{\frac{K-k}{10K}} \tag{4.6}$$

where α, β, γ, η, and b are the convergent parameters. K is the total number of

elements in one of the corridors, which are formed by space-charge-free field lines from dc conductor nodes to the ground nodes. The value of k is determined by the relative position of an element in a corridor, which starts at 1 for elements adjacent to the dc conductor and increases linearly to K for the elements adjacent to the ground level. The last term ensures that the correction to enforce the Kaptzov's boundary condition has a greater effect near the dc conductor.

By using the same trial-and-error procedure as for Geometry 1, it was found that the convergence could be achieved for the following values of the parameters: α between -2.5 and -0.8, β between -1.5 and -0.5, η between -1.0 and -0.2, γ between -1.2 and 0.5, and b between 1.5 and 3.5. The optimum values depend on the geometry and/or the mesh. For Geometries 2 & 3, the solutions were obtained for α = -1.0, β = -0.5, η = -0.25, b = 2.5, and γ = -0.5. For Geometry 4, the same values of the parameters were used, except b = 2.0 and γ = 0.0. For Geometry 5, the same values as in Geometries 2 & 3 were used, except b = 2.0 and γ = -0.5.

It can be seen from the two update algorithm Equations (4.5) and (4.6) that upon convergence, i.e., when $\Phi_{1i} \approx \Phi_{2i}$, $E_{1i} \approx E_{2i}$, $E_{1j} \approx E_{2j} \approx E_o$, the correction to ρ tends to vanish and $\rho_{newi} \approx \rho_{oldi}$.

4.4 COMPUTED RESULTS AND ANALYSIS

4.4.1 Comparison of the Computed Results with Experimental Data for Geometry 1

The computed results for the laboratory line are based on the solutions of the time-invariant ionized field problem described before, i. e., V_{ac}=0. The effect of the ac voltages is included by replacing the dc voltage with an equivalent voltage V_{eq}, which is obtained by keeping the maximum space-charge-free field intensity constant on the dc conductor surface irrespective of the ac voltages [4]. By the method of images described in Subsection 3.3.1, the relationship between the maximum field intensity on the dc conductor surface, which occurs when the ac voltage is set to its maximum negative value, and the applied dc and ac voltages can be expressed as

$$E_{max} = 1.71\ V_{dc} + 0.57\ V_{ac} \tag{4.6}$$

where V_{dc} = 60 kV and V_{ac} is the RMS value of the ac voltage, which is 10 kV, 20 kV, and 25 kV, respectively. When V_{ac} = 10 kV, E_{max} equals 108.19 kV/cm from Equation (4.6). Setting V_{ac} at zero potential and keeping E_{max} unchanged, the equivalent dc voltage can be obtained by replacing V_{dc} by V_{eq} in Equation (4.6), i.e., V_{eq} = 63.35 kV. Replacing V_{dc} by V_{eq} in the iterative FEM, the ionized field problem can be solved corresponding to V_{ac} = 10 kV. Similarly, the effect of ac voltage of 20 kV and 25 kV can also be simulated in the same manner.

Figures 4.3 - 4.6 show the comparison of the computed results with the experimental ones for V_{ac}=0, 10 kV, 20 kV, and 25 kV, respectively. The results agree quite well

for V_{ac}=10 and 20 kV. However, when V_{ac}=0, the position of the peak value of the current density at ground level calculated by FEM does not agree well with the experimental data, as shown in Figure 4.3. This is due to the fact that the ac conductor is replaced by a line charge when the method of images is applied to calculate the space-charge-free field. Consequently, the dimension of the ac conductor, which may have some shielding effect on the ionized field, has been neglected.

With the increase of ac voltages, the calculated values of the current density (J) increase as shown in Figure 4.7, whereas the measured values have a tendency of decrease as shown in Figure 4.8. The reason for this is that when the ac voltage is increased above a certain value, the ac conductors will be in corona too. This phenomena, however, is very difficult to simulate by the FEM. This explains the bigger differences between the calculated and the measured values in Figure 4.6.

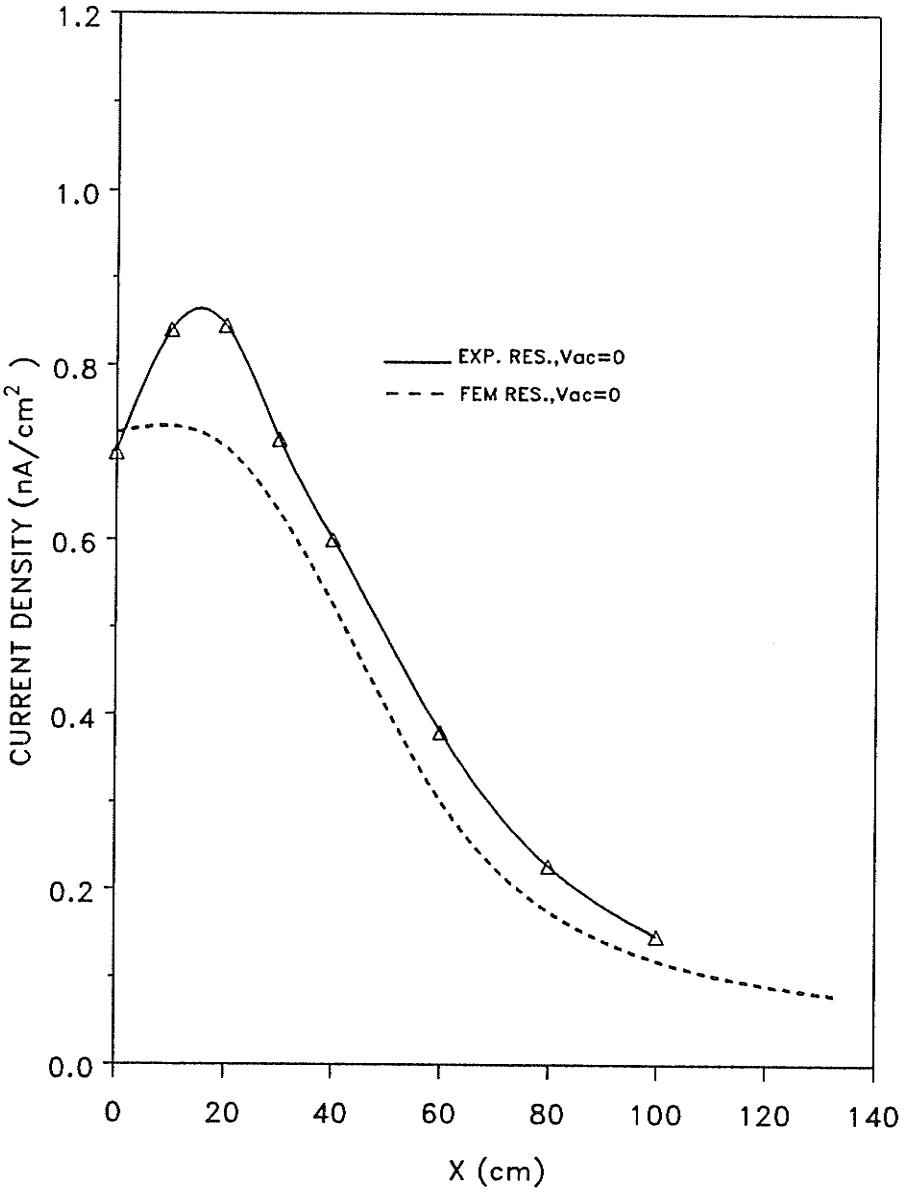

Figure 4.3: *Current Density Profile at Ground Level for Geometry 1,* V_{ac}*=0,* V_{dc}*=60kV*

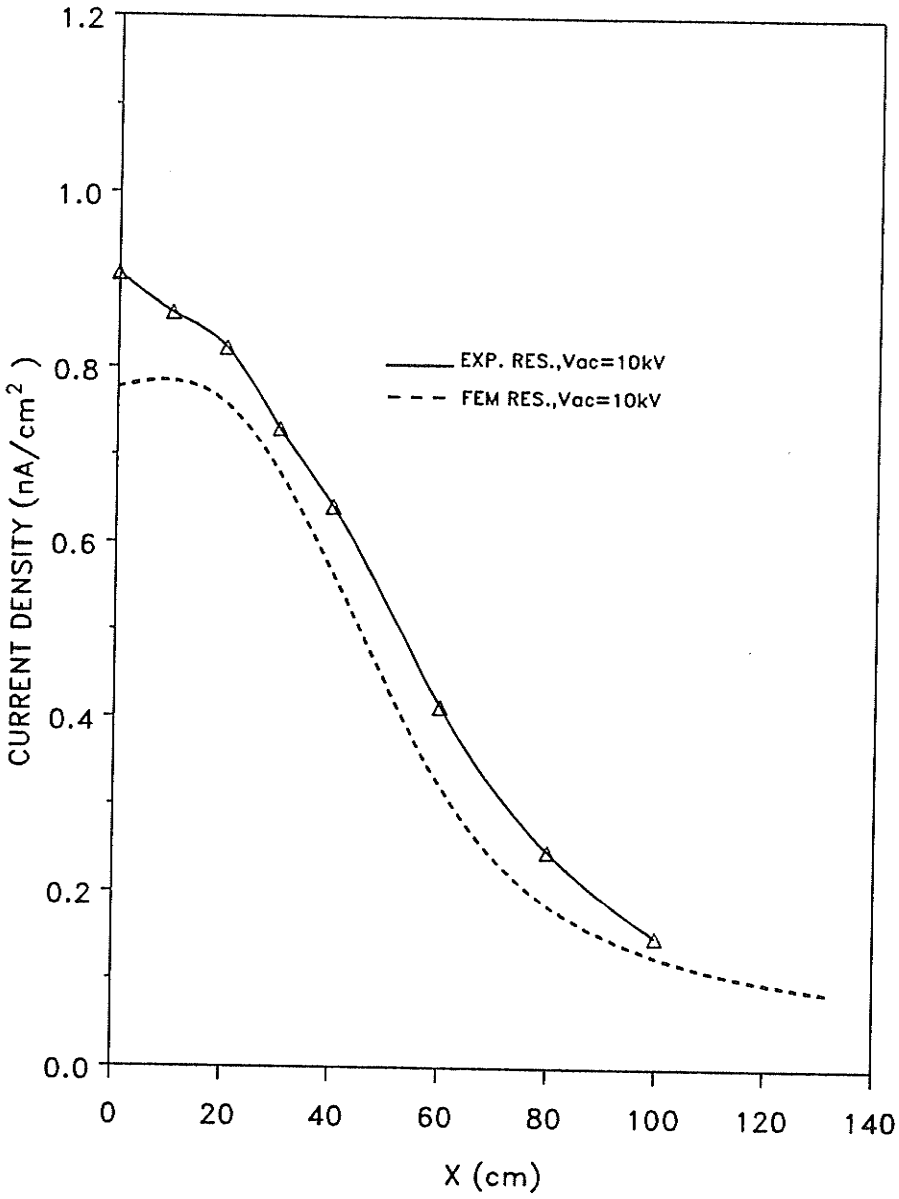

Figure 4.4: *Current Density Profile at Ground Level for Geometry 1, V_{ac}=10 kV, V_{dc}=60 kV*

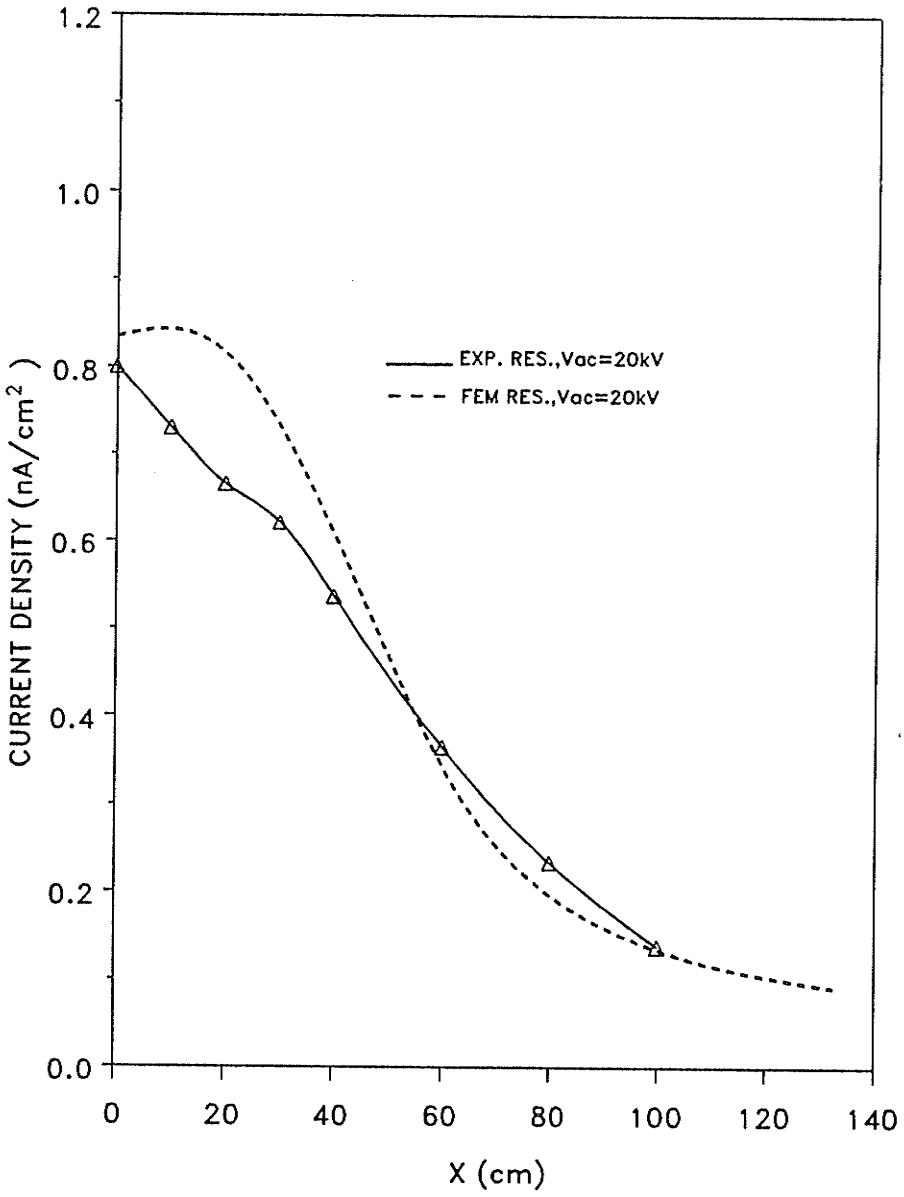

Figure 4.5: *Current Density Profile at Ground Level for Geometry 1, V_{ac}=20 kV, V_{dc}=60 kV*

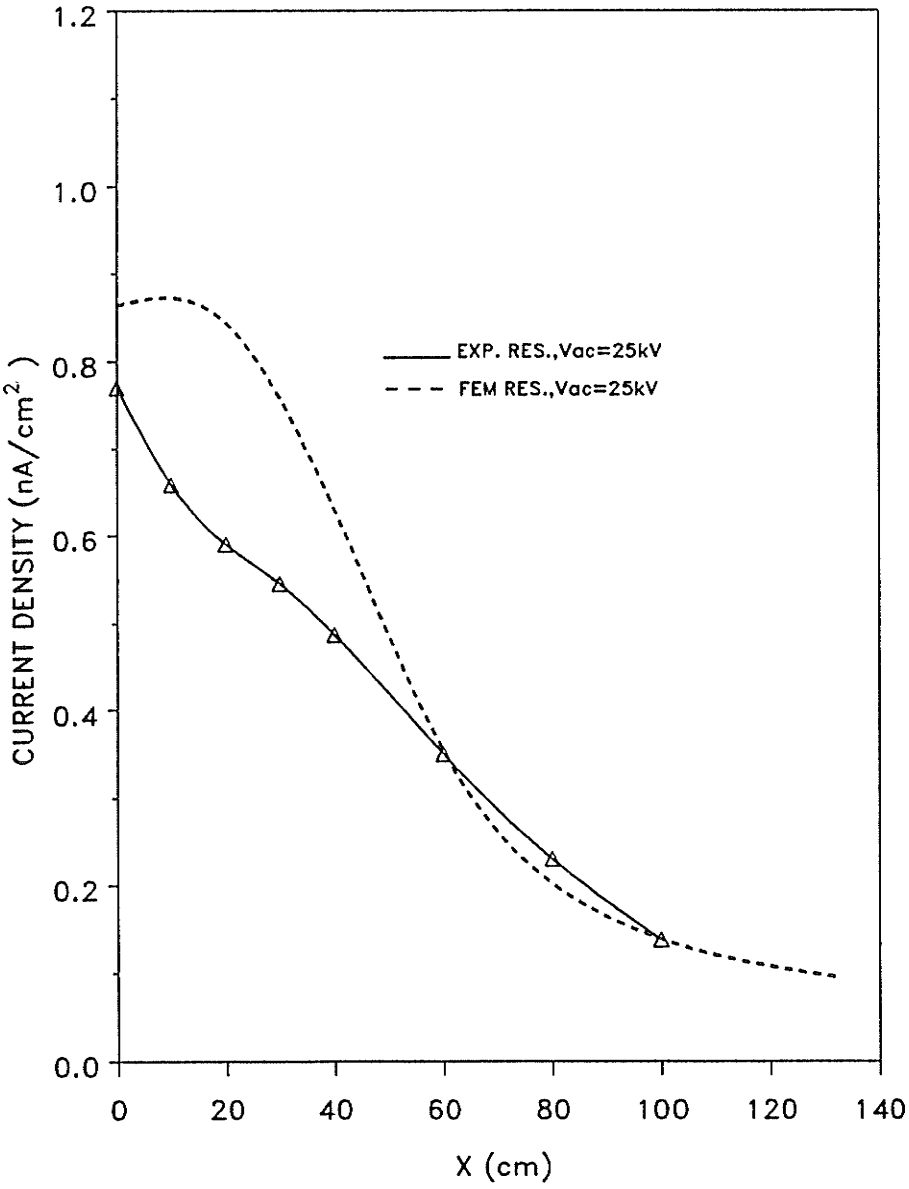

Figure 4.6: *Current Density Profile at Ground Level for Geometry 1, V_{ac}=25 kV, V_{dc}=60 kV*

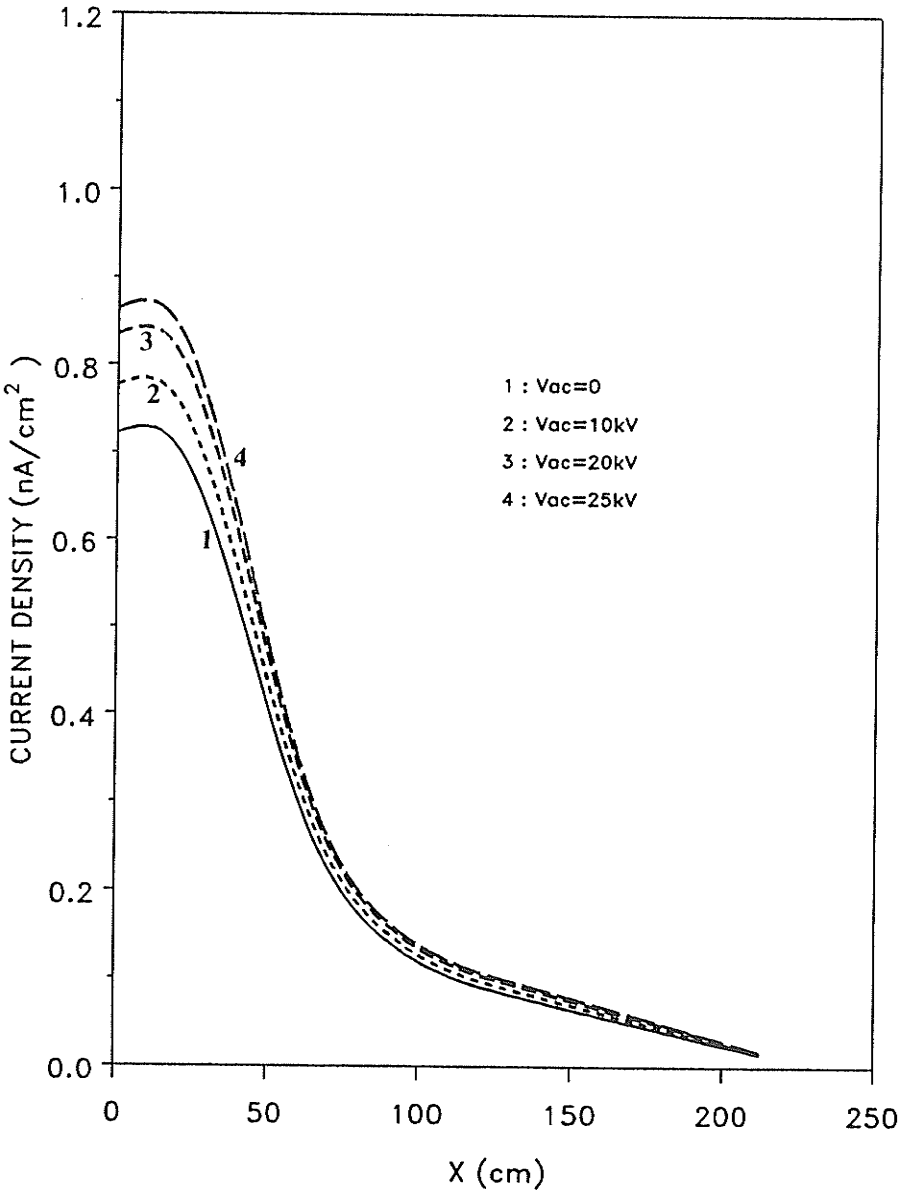

Figure 4.7: *Current Density Profiles at Ground Level by FEM for Geometry 1, V_{ac}=0,10, 20,and 25 kV, V_{dc}=60 kV*

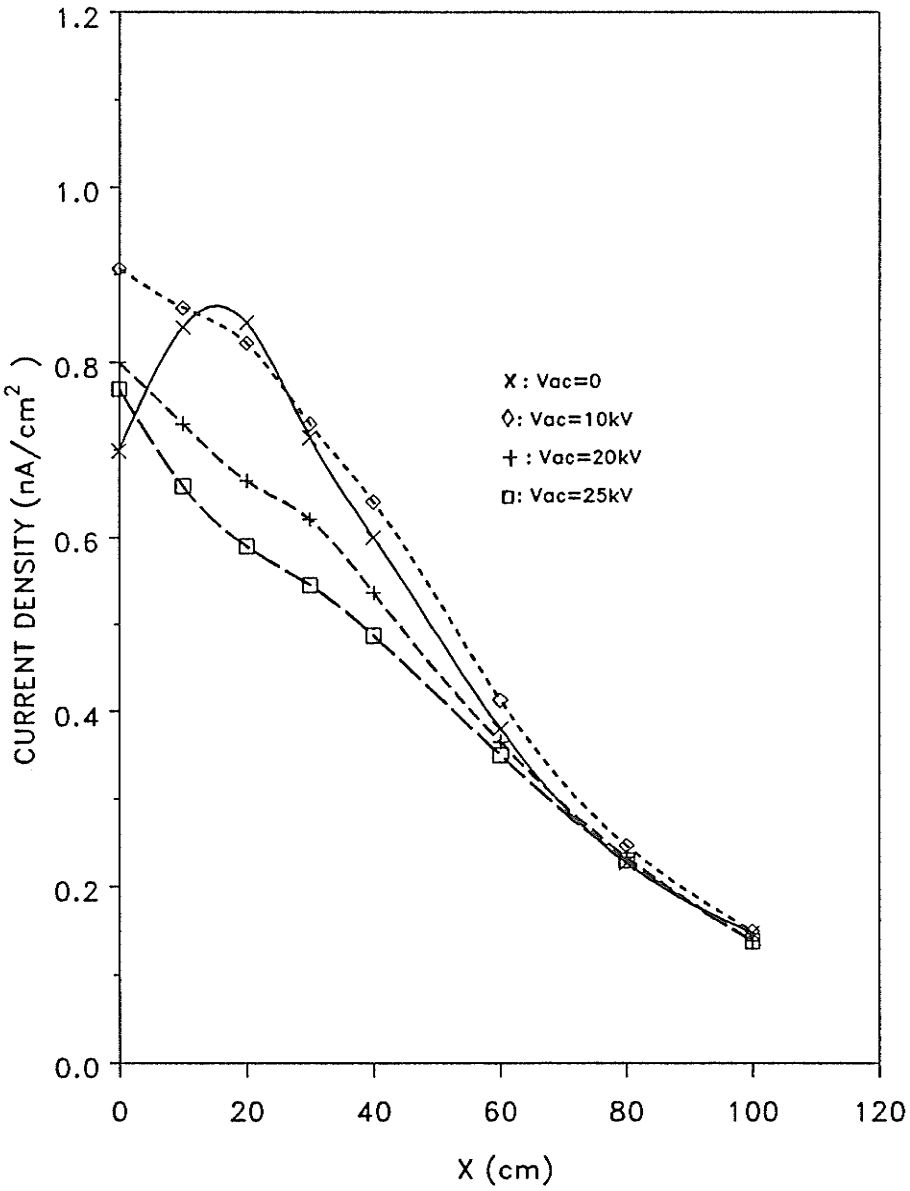

Figure 4.8: *Current Density Profiles at Ground Level by Experiments for Geometry 1, V_{ac}=0,10, 20,and 25 kV, V_{dc}=60 kV*

4.4.2 Computed Results for Geometries 2 to 5

The purpose here is to analyze the effects of hybrid line geometries on the corresponding lateral profiles of the electric field intensity and the current density at ground level from point of view of environmental impact. For simplicity, the ac conductors are assumed to be at zero potential only.

The ground level lateral profiles of electric field intensity and current density for Geometries 2 to 5 are shown in Figures 4.9(a) to 4.11(a) and 4.9(b) to 4.11(b), respectively. In Geometry 3, the maximum electric field intensity and current density are reduced by 4% and 17% respectively, compared with Geometry 5. By comparing Figure 4.9 (a) & (b) with Figure 4.11 (a) & (b), respectively, it can be seen that Geometry 2 does not show the obvious shielding effect of the ac conductors, whereas its influence is much more pronounced for Geometry 4 where the maximum electric field intensity and current density are reduced by 11% and 32%, respectively, compared with Geometry 5. The reason is that when outer phase ac conductors are relatively close to the center phase as compared with the distance between the bipolar dc conductors (Geometry 2), the area screened by the ac conductors is within the problem domain when the ac lines are not present (Geometry 5). However, the dc corona activities are increased by lifting the zero potential from ground to the position of the ac conductors. When the outer phases of ac lines are moved further apart from the center phase (Geometry 4), the area screened by the ac lines increases and the electric quantities (E, ρ, J) at ground level therefore decrease.

By comparing Figure 4.10 (a) & (b) and Figure 4.11 (a) &(b) with Figure 4.9 (a) &

(b), respectively, it can be seen that the maximum electric field intensity and current density at ground level in Geometry 3 are reduced by 4% and 14%, respectively, compared with the ones in Geometry 2; the ones in Geometry 4 are reduced by 11% and 29%, respectively, compared with the ones in Geometry 2.

It can be concluded that with a proper ac line arrangement, the hybrid line geometries have the advantage for reducing the electric field intensity and current density to values lower than those which would be expected by increasing the height of the dc conductors alone.

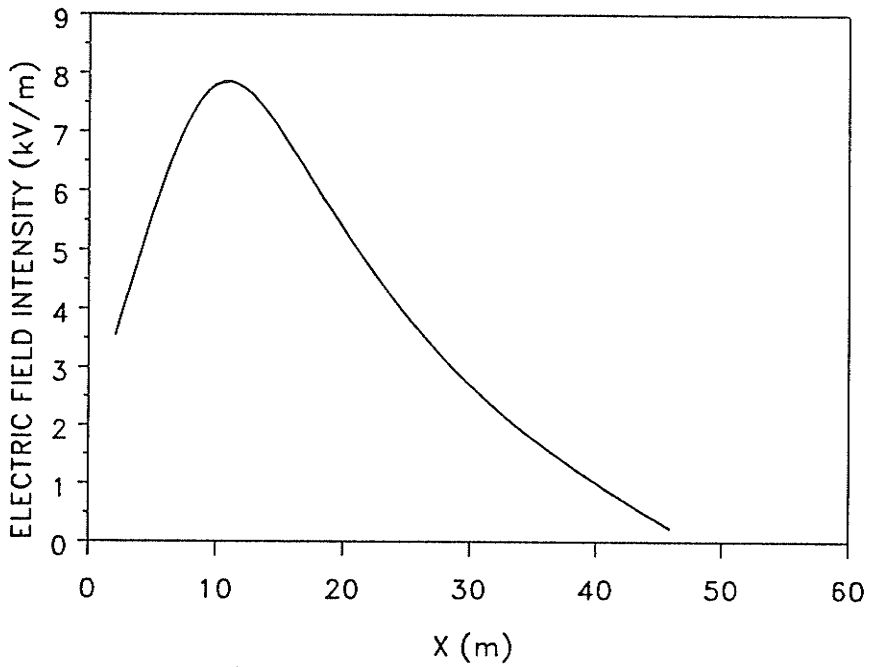

Figure 4.9 (a): *Lateral Profile of Electric Field Intensity at Ground Level, Geometry 2, V_{ac}=0, V_{dc}=300 kV*

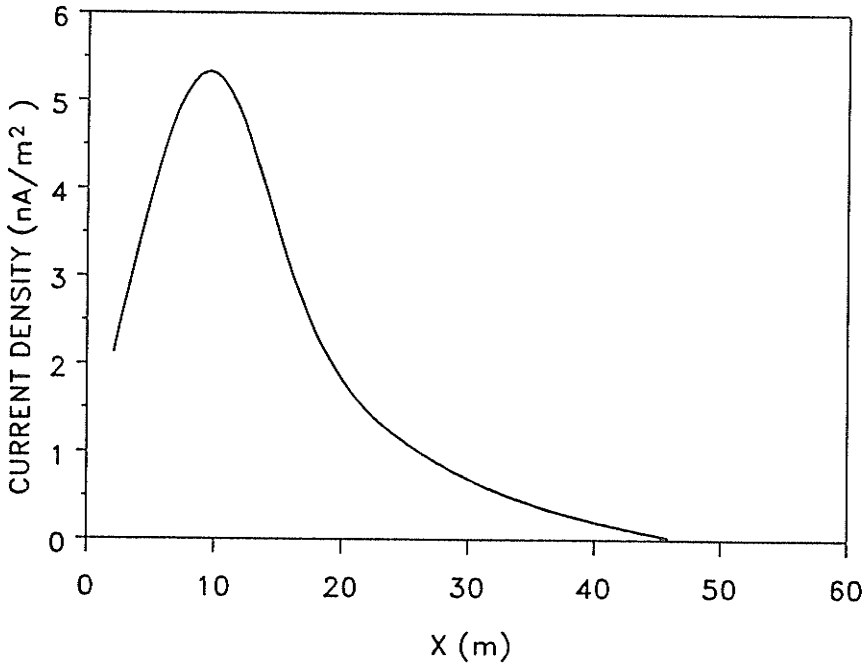

Figure 4.9 (b): *Lateral Profile of Current Density at Ground Level, Geometry 2, V_{ac}=0, V_{dc}=300 kV*

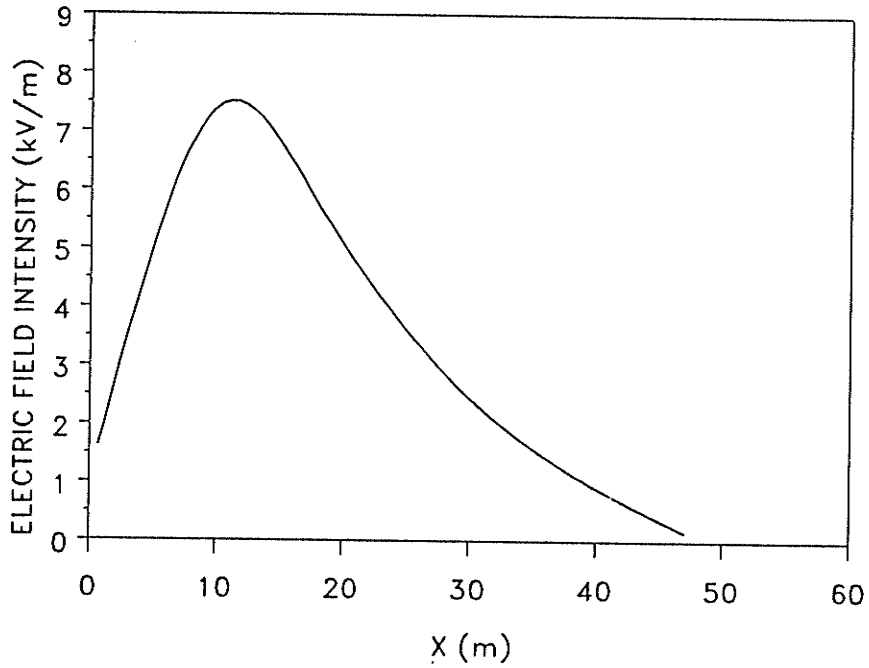

Figure 4.10 (a): *Lateral Profile of Electric Field Intensity at Ground Level,Geometry 3, V_{ac}=0, V_{dc}=300 kV*

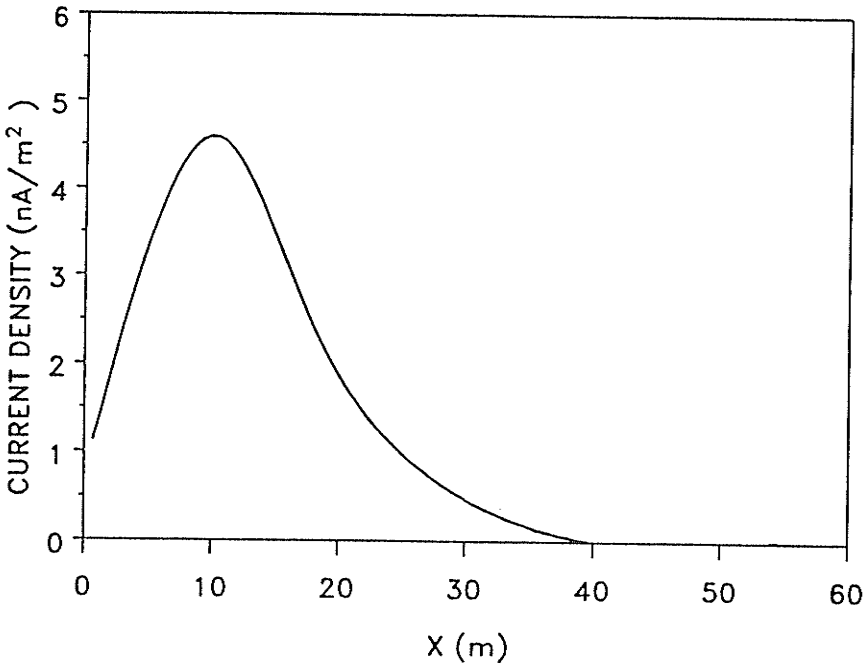

Figure 4.10 (b): *Lateral Profile of Current Density at Ground Level, Geometry 3, V_{ac}=0, V_{dc}=300 kV*

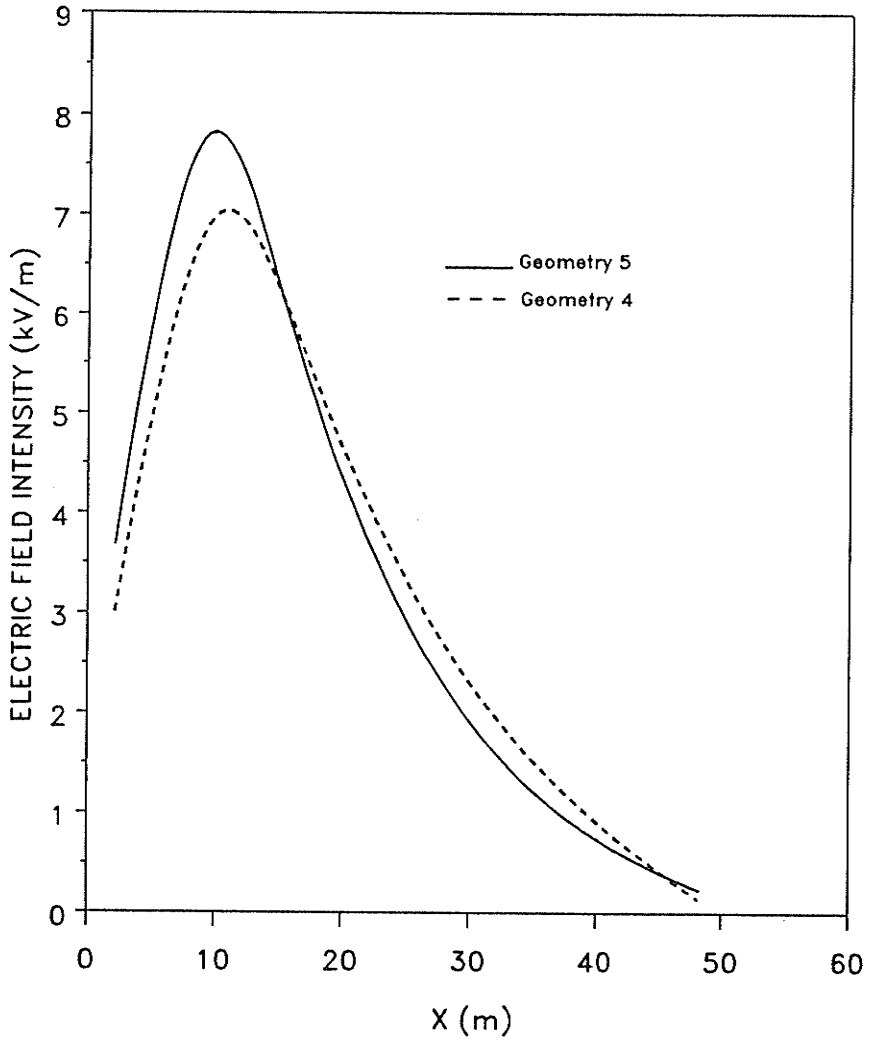

Figure 4.11 (a): *Lateral Profiles of Electric Field Intensity at Ground Level, Geometries 4 & 5, V_{ac}=0, V_{dc}=300 kV*

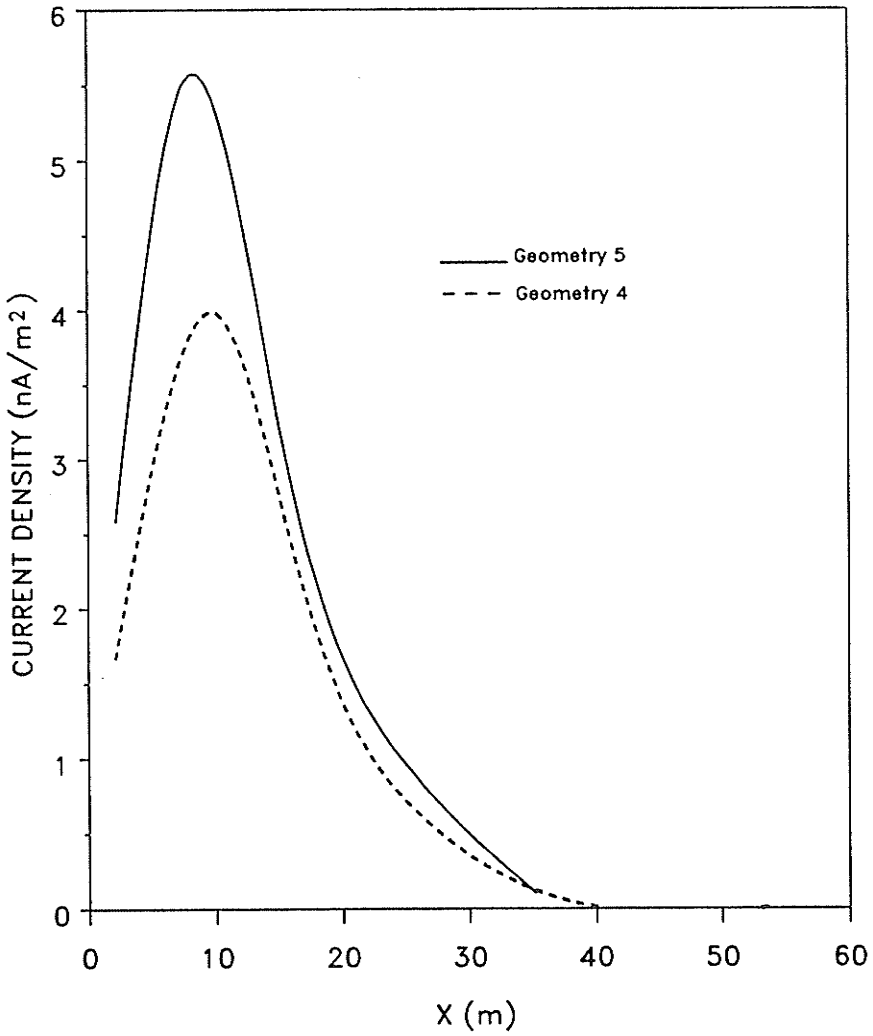

Figure 4.11 (b): *Lateral Profiles of Current Density at Ground Level, Geometries 4 & 5, V_{ac}=0, V_{dc}=300 kV*

Chapter 5
CONCLUSIONS

An iterative FE program has been developed and applied to different geometries in this work. The procedures for constructing the finite element mesh and approximating the initial space charge distribution have also been presented. Initially, the program was checked by applying it to the case of a coaxial cylindrical configuration, then extended to four hybrid ac/dc geometries and one bipolar dc geometry.

The iterative FEM works very well in converging to a solution of the ionized field problems even with significantly inaccurate initial approximations for the space charge distribution. Comparison of the calculated results of the ionic current density at ground level for the single-phase laboratory ac/dc configuration (Geometry 1) with available experimental data showed satisfactory agreement.

The calculated results of the ground level lateral profiles of electric field intensity and the current density for the various practical hybrid ac/dc transmission lines have also been obtained. For further discussion of the shielding effect of the ac conductors on the electric environment, the lateral profiles of electric field intensity and the current density for the bipolar geometry (Geometry 5) have also been calculated. It can be

concluded that with a proper arrangement of the ac circuit in a hybrid ac/dc line configuration, there is a significant shielding effect of the ac conductors on the ionized field intensity and the current density at ground level. The hybrid ac/dc lines have the advantage for reducing the electric quantities to the values lower than those by increasing the height of the dc conductors alone.

Based on the research work carried out in this thesis, it is recommended that the present analysis be extended to the case of bundled hybrid ac/dc transmission lines. In addition, it was found that the final values for the space charge distribution at ground level were different when the initial approximations were different even through convergence of solution was reached as specified. It is recommended that an improved analysis by employing the space charge density on the coronating conductor surface as the third boundary condition be developed in the future to ensure the unique solutions not only for the ionized field but also for the final space charge distribution.

REFERENCES

1. V. L. Chartier, S. H. Sarkinen, R. D. Stearns, and A. L. Burns, "*Investigation of Corona and Field Effects of AC/DC Hybrid Transmission Lines*", IEEE Transactions on Power Apparatus and Systems, Vol. PAS-100, No. 1, Jan. 1981, pp. 72-80

2. H. L. Nadra, L. X. Bui, and L. Lyoda, "*System Considerations in Converting One Circuit of a Double Circuit AC Line to DC*", IEEE Transactions on Power Apparatus and Systems, Vol. PAS-103, No. 10, Oct. 1984, pp. 3096-3103

3. P. Sarma Maruvada and S. Drogi, "*Field and Ion Interaction of Hybrid AC/DC Transmission Lines*", IEEE Transactions on Power Delivery, Vol. 3, No. 3, Jul. 1988, pp. 1165-1172

4. A. F. Penner, "*Finite Element Computation of the DC Corona Currents Injected into the AC Conductors of a Hybrid AC/DC Transmission Line*", Master Thesis, University of Manitoba, 1989

5. M. R. Raghuveer, "*Laboratory Investigation of Hybrid ac/dc Transmission System Corona Performance*",Journal of Electrostatics, No. 22, 1989, pp. 279-288.

6. Maruvada P. Sarma, R. D. Dallaire, O. C. Norris-Elye, and C.V. Thio, J. S. Goodman, *"Environmental Effects of the Nelson River HVDC Transmission Line - RI, AN, Electric Field, Induced Voltage, and Ion Current Distribution Tests"*, IEEE Transactions on Power Apparatus and Systems, Vol. PAS-101, No. 4, April 1982, pp. 951 - 959

7. Maruvada P. Sarma, *"Corona-Generated Space Charge Environment in the Vicinity of HVDC Transmission Lines"*, IEEE Transactions on Electrical Insulation, Vol. EI - 17, No. 2, April 1982, pp. 125 - 130

8. W. Janischewskyj, Maruvada P. Sarma, and G. Gela, *"Corona Losses and Ionized Fields of HVDC Transmission Lines"*, CIGRE 36.09, 1982, 10

9. J. S. Townsend, "*The Potentials Required to Maintain Currents between Coaxial Cylinders*", Philosophical Magazine and Journal of Science, Series 6, Vol. 28, 1914, pp. 83-90

10. W. Deutsch, "*Uber Die Dichtverteilung Unipolarer Ionenstrome*", Annalen der Physik, Vol. 5,1933, pp. 589-613

11. V. I. Popkov, "*On the Theory of Unipolar DC Corona*", Eleckrichestvo, (1): 33-48, 1949, NRC Technical Translation - 1093

12. V. I. Popkov, "*Some Special Features of Corona on High-Voltage DC Transmission Lines*", in Gas Discharges and the Electricity Supply Industry. London: Butterworth, 1962

13. Maruvada P. Sarma and W. Janischewskyj, "*Analysis of Corona Losses on DC Transmission Lines: I - Unipolar Lines*", IEEE Transactions on Power Apparatus and Systems, Vol. PAS-88, No. 5, May 1969, pp. 718-731

14. Maruvada P. Sarma and W. Janischewskyj, "*Analysis of Corona Losses on DC Transmission Lines: II - Bipolar Lines*", IEEE Transactions on Power Apparatus and Systems, Vol. PAS-88, No. 10, Oct. 1969, pp. 1476-1491

15. M. D'Amore, V. Daniele, and G. Ghione, "*New Analytical Approach for Computing DC Unipolar Corona Losses*", Proceeding IEE, Vol. 131, July 1984, pp. 318-324

16. P. Atten, "*Etude Mathematique du Probleme du Champ Electrique Affecte par un Flux Permanent d'Ions Unipolaires et Application a la Theorie de la Sonde Froide*", Doctoral Thesis, Faculty of Science, University of Grenoble, Nov. 1969

17. T. Takuma, T. Ikeda, and T. Kawamoto, "*Calculation of Ion Flow Fields of HVDC Transmission Lines by the Finite Element Method*", IEEE Transactions on Power Apparatus and Systems, Vol. PAS-100, No. 12, Dec.

1981, pp. 4802-4810

18. M. Abdel - Salam, M. Farghally, and S. Abdel - Sattar, "*Monopolar Corona on Bundle Conductors*", IEEE Transactions on Power Apparatus and Systems, Vol. PAS-101, No. 10, Oct. 1982, pp. 4079-4088

19. Y. Sunaga and U. Sawada, "*Method of Calculating Ionized Field of HVDC Transmission Lines and Analysis of Space Charge Effects on RI*", IEEE Transactions on Power Apparatus and Systems, Vol. PAS-99, No. 2, May 1980, pp. 605-615

20. M. Khalifa and M. Abdel - Salam, "*Improved Method for Calculating DC Corona Losses*", IEEE Transactions on Power Apparatus and Systems, Vol. PAS-93, 1974, pp. 720-726

21. W. Janischewskyj and G. Gela, "*Finite Element Solution for Electric Fields of Coronation DC Transmission Lines*", IEEE Transactions on Power Apparatus and Systems, Vol. PAS-98, No. 3, May/June 1979, pp. 1000-1012

22. M. Abdel - Salam, M. Farghally, and S. Abdel - Sattar, "*Finite Element Solution of Monopolar Corona Equation*", IEEE Transactions on Electrical Insulation, Vol. EI-18, No. 2, April 1983, pp. 110-119

23. R. T. Waters, T. E. Rickard, and W. B. Stark, "*Electric Field Measurements in DC Discharges*", IEE Conf. Pub. 90, 1972, pp. 188-190

24. M. Khalifa and M. Abdel - Salam, "*Calculating the Surface Fields of Conductors in Corona*", Proceeding IEE, 1973, pp. 1574-1575

25. I. R. Ciric and M. R. Raghuveer, "*Calculation of Coronating Conductor Surface Fields from Ground Level Experimental Data*", 5th ISH, Braunschweig, 24-28 Aug. 1987, Paper 32.03

26. H. Singer, H. Steinbigler, and P. Weiss, "*A Charge Simulation Method for the Calculation of HV Fields*", IEEE Transactions on Power Apparatus and Systems, Vol. PAS-93, 1974, pp. 1660-1668

27. M. Khalifa, M. Avdeo - Salam, F. Ali, and M. Abon-Seada, "*Electric Fields around Conductor Bundles of EHV Transmission Lines*", IEEE PES paper No. A-75-563-7, 1975

28. M. N. Horensitein, "*Computation of Corona Space Charge and V-I Characteristics Using Equipotential Charge Shells*", Proceeding of the IEEE-IAS Annual Meeting, 1983, pp. 974-981

29. B. L. Qin, J. N. Sheng, Z. Yan, and G. Gela, "*Accurate Calculation of Ion Flow Field under HVDC Bipolar Transmission Lines*", IEEE Transactions on Power Apparatus and Systems, Vol. PAS-3, No. 1, Jan. 1988, pp. 368-376

30. M. Abdel-Salam and S. Abdel-Sattar, "*Calculation of Corona V-I Characteristics of Monopolar Bundles Using the Charge Simulation Method*", IEEE Transactions on Electrical Insulation, Vol. 24, No. 4, August 1989,

pp.669 - 679

31. M. Friedman, D. J. Richards, W. N. R. Stevens, and A. Wexler, "*MANFEP, User's Manual*", Dept. of Elec. Eng., Univ. of Manitoba, Winnipeg, Canada, 1979

32. Bonneville Power administration, "*Transmission Line Reference Book - HVDC to ± 600 kV*", Electrical Power Research Institute, Palo Alto, CA., 1977

33. Lambert, "*Computational Methods in Ordinary Differential Equations*", John Wiley and Sons Ltd., London, 1973

34. G. Gela, "*Computation of Ionized Fields Associated with Unipolar DC Transmission Systems*", Ph.D. thesis, Dept. of Elec. Eng., Univ. of Toronto, April 1980

Appendix A
MISCELLANEOUS EQUATIONS

A.1 DETERMINATION OF SPACE-CHARGE-FREE FIELDS BY THE METHOD OF IMAGES

A.1.1 Solutions for Geometry 1

$$V_{eq} = Q_1 \ln \frac{2H_1}{r} + Q_2 \ln \frac{H_1 + H_2}{H_1 - H_2} = Q_1 C + Q_2 B$$

$$V_{ac} = Q_1 \ln \frac{H_1 + H_2}{H_1 - H_2} + Q_2 \ln \frac{2H_2}{r} = Q_1 B + Q_2 A = 0$$

where $A = \ln \frac{2 H_2}{r}$, $B = \ln \frac{H_1 + H_2}{H_1 - H_2}$, and $C = \ln \frac{2 H_1}{r}$.

Let $DET = \begin{vmatrix} C & B \\ B & A \end{vmatrix} = A C - B^2$, now we have $Q_1 = A \frac{V_{eq}}{DET}$, $Q_2 = - B \frac{V_{eq}}{DET}$.

The potential at any point (x, y) can be expressed as,

$$\Phi(x, y) = \frac{Q_1}{2} \ln \frac{x^2 + (y + H_1)^2}{x^2 + (y - H_1)^2} + \frac{Q_2}{2} \ln \frac{x^2 + (y + H_2)^2}{x^2 + (y - H_2)^2}$$

The magnitude of the space-charge-free field intensity at any point (x, y) is,

$$E = \sqrt{E_x^2 + E_y^2}$$

where

$$E_x = E_{x1} + E_{x2} + E_{x3} + E_{x4}, \qquad E_y = E_{y1} + E_{y2} + E_{y3} + E_{y4}$$

$$E_{x1} = \frac{Q_1 x}{(H_1 - y)^2 + x^2}, \qquad E_{y1} = \frac{-Q_1 (H_1 - y)}{(H_1 - y)^2 + x^2}$$

$$E_{x2} = \frac{Q_2 x}{(H_2 - y)^2 + x^2}, \qquad E_{y2} = \frac{-Q_2 (H_2 - y)}{(H_2 - y)^2 + x^2}$$

$$E_{x3} = \frac{-Q_2 x}{(H_2 + y)^2 + x^2}, \qquad E_{y3} = \frac{-Q_2 (H_2 + y)}{(H_2 + y)^2 + x^2}$$

$$E_{x4} = \frac{-Q_1 x}{(H_1 + y)^2 + x^2}, \qquad E_{y4} = \frac{-Q_1 (H_1 + y)}{(H_1 + y)^2 + x^2}$$

A.1.2 Solutions for Geometries 2 to 4

$$V_{dc} = Q_1 \left[\ln \frac{2 H_1}{r_{dc}} + \frac{1}{2} \ln \frac{(2 S_1)^2 + r_{dc}^2}{(2 S_1)^2 + (2 H_1)^2} \right] + \frac{Q_2}{2} \ln \frac{S_1^2 + (H_1 + H_2)^2}{S_1^2 + (H_1 - H_2)^2}$$

$$+\frac{Q_3}{2}\left[\ln\frac{(S_1 - S_3)^2+(H_1 + H_3)^2}{(S_1 - S_3)^2+(H_1 - H_3)^2}+\ln\frac{(S_1 + S_3)^2+(H_1 - H_3)^2}{(S_1 + S_3)^2+(H_1 + H_3)^2}\right]$$

$$0 = Q_2 \ln\frac{2H_2}{r_{ac}}$$

$$0 = \frac{Q_1}{2}\left[\ln\frac{(S_1 - S_3)^2+(H_1 + H_3)^2}{(S_1 - S_3)^2+(H_1 - H_3)^2}-\ln\frac{(S_1 + S_3)^2+(H_1 + H_3)^2}{(S_1 + S_3)^2+(H_1 - H_3)^2}\right]$$

$$+\frac{Q_2}{2}\ln\frac{S_3^2+(H_1 + H_2)^2}{S_3^2+(H_1 - H_2)^2}+Q_3\left[\ln\frac{2H_3}{r_{ac}}+\frac{1}{2}\ln\frac{(2S_3)^2+r_{ac}^2}{(2S_3)^2+(2H_3)^2}\right]$$

$$\Rightarrow Q_1 = A\cdot\frac{V_{dc}}{DET}\ ,\ Q_2 = 0,\ \text{and}\ Q_3 = -B\cdot\frac{V_{dc}}{DET}\ ,\ \text{where DET} = A\cdot C - B^2\ ,$$

$$A = \ln\frac{2H_3}{r_{ac}}+\frac{1}{2}\ln\frac{(2S_3)^2+r_{ac}^2}{(2S_3)^2+(2H_3)^2}\ ,$$

$$B = \frac{1}{2}\left[\ln\frac{(S_1 - S_3)^2+(H_1 + H_3)^2}{(S_1 - S_3)^2+(H_1 - H_3)^2}-\ln\frac{(S_1 + S_3)^2+(H_1 + H_3)^2}{(S_1 + S_3)^2+(H_1 - H_3)^2}\right]$$

$$C = \ln\frac{2H_1}{r_{dc}}+\frac{1}{2}\ln\frac{(2S_1)^2+r_{dc}^2}{(2S_1)^2+(2H_1)^2}$$

Then the potential at any point (x, y) is given by,

$$\Phi(x, y) = \frac{Q_1}{2}\left[\ln \frac{(x_1 - S_1)^2 + (y + H_1)^2}{(x_1 - S_1)^2 + (y - H_1)^2} \times \frac{(x_1 + S_1)^2 + (y - H_1)^2}{(x_1 + S_1)^2 + (y + H_1)^2} \right]$$

$$+ \frac{Q_3}{2}\left[\ln \frac{(x_1 - S_3)^2 + (y + H_3)^2}{(x_1 - S_3)^2 + (y - H_3)^2} \times \frac{(x_1 + S_3)^2 + (y - H_3)^2}{(x_1 + S_3)^2 + (y + H_3)^2} \right]$$

and the magnitude of the space-charge-free field intensity is,

$$E = \sqrt{E_x^2 + E_y^2} \ ,$$

where E_x is the sum of x component of the electric field of each line charge including the imaged ones, E_y is the sum of y component of the electric field of each line charge including the imaged ones.

A.1.3 Solutions for Geometry 5

$$V_{dc} = Q_1\left[\ln \frac{2 H_1}{r_{dc}} + \frac{1}{2} \ln \frac{(2 S_1)^2 + r_{dc}^2}{(2 S_1)^2 + (2 H_1)^2} \right] = Q_1 C \ ,$$

where $$C = \ln \frac{2 H_1}{r_{dc}} + \frac{1}{2} \ln \frac{(2 S_1)^2 + r_{dc}^2}{(2 S_1)^2 + (2 H_1)^2}$$

$$\Rightarrow Q_1 = \frac{V_{dc}}{C}$$

Then the potential at any point (x, y) is given by,

$$\Phi(x, y) = \frac{Q_1}{2}\left[\ln \frac{(x_1 - S_1)^2 + (y + H_1)^2}{(x_1 - S_1)^2 + (y - H_1)^2} \times \frac{(x_1 + S_1)^2 + (y - H_1)^2}{(x_1 + S_1)^2 + (y + H_1)^2} \right]$$

and the magnitude of the space-charge-free field intensity is,

$$E = \sqrt{E_x^2 + E_y^2} \ ,$$

where E_x and E_y have the same definitions as in A.1.2.

A.2 ANALYTICAL SOLUTIONS FOR THE IONIZED FIELD IN COAXIAL CYLINDER GEOMETRY

For the case depicted in Fig. 3.11, the analytical solutions for Φ, E, and ρ in the region of interest (r_c, r_g) are given by the following closed form equations by Gela [17],

$$\Phi(r) = V_c - K_1\left\{ f_1(r) - K_2 + K_3\left[\ln \frac{r}{r_c} + \ln (K_3 + K_2) - \ln (K_3 + f_1(r)) \right] \right\} \quad \text{(A.2.1)}$$

$$E(r) = \frac{K_1}{r} f_1(r) \quad \text{(A.2.2)}$$

$$\rho(r) = \frac{\sqrt{r_c E_o \varepsilon_o \rho_0}}{f_1(r)} \quad \text{(A.2.3)}$$

where

$$K_1 = \frac{\sqrt{r_c E_o \rho_0}}{\varepsilon_o} \ , \qquad f_1(r) = \sqrt{r^2 + K_2^2 - r_c^2} \ ,$$

$$K_2 = \frac{\sqrt{r_c E_o \varepsilon_o}}{\rho_0} \quad , \qquad K_3 = \sqrt{K_2^2 - r_c^2} \quad ,$$

and $\rho_0 = \rho\ (r_c)$ determined implicitly by the following equation,

$$V_c = K_1\left\{f_1(r_g) - K_2 + K_3\left[\ln\frac{r_g}{r_c} + \ln\left(K_3 + K_2\right) - \ln\left(K_3 + f_1(r_g)\right)\right]\right\} \qquad \text{(A.2.4)}$$

Appendix B
PROGRAM LISTING

B.1 MESH GENERATION PROGRAM

```
//WANG JOB ',,,T=2M,L=35,I=20','DC-AC FEPMAP',CLASS=1
// EXEC WATFIV,SIZE=2048K
//SYSIN DD *
$JOB  WATFIV   WANG,NOEXT
C
C  DETERMINING A FE MESH FOR THE FIVE CONDUCTOR PROBLEM
C
      IMPLICIT REAL*8 (A-H,O-Z)
       REAL*8 TH,VDC,VAC,TSTEP,H1,H2,R,PHI,THS,THM,TD,PI,TNW(800,3),
     & X(28000),Y(28000),D(28000),XN(200),YN(200),A,B,C,DET,W,TH2,TNMIN,
     & TNMAX,G,XA(100),YA(100),XS(2000),YS(2000),DI,P(800),XP(500),
     & YP(500),TN(200),ROE(200),T(28000),DL(200)
       INTEGER NL,NN(20),NP,I,J,K,L,M,IT(800,3),NT,NL1
       COMMON A,B,C,DET,VDC,VAC,H1,H2,W,H3,S1,S3
C
C       THM=111.0-69.0
C2       THM=108.0-66.0
      THM=106.0-63.0
      VDC=300000.0
      VAC=0.0D0
      DI=4.0D-6
      TSTEP=0.0000001
      PI=3.141592653
C2       H1=16.34
      H1=17.34
      S1=4.57
      H2=14.20
      H3=12.38
      S3=5.49
```

```
C      S3=6.49
       RDC=0.01755
       RAC=0.01599
       L=0
       W=60.0*PI
       TNMIN=0.0000001
       TNMAX=0.000001
       G=1.4
       NL=5
C      NL=4
       NL1=NL-1
       THS=THM/NL1
C
       DO 10 I=1,NL
         TH=THS*(I-1)+63.0
         CALL RKP(TH,TSTEP,RDC,NP,TD,X,Y,T,D,TNMIN,TNMAX)
C
         CALL PATH(TSTEP,NP,TD,NN(I),XN,YN,TN,DL,RDC,X,Y,T,D,G,I)
C          CALL INROE(TH,RDC,PI,XN,YN,TN,NN(I),ROE)
       CALL CINROE(TH,RDC,PI,XN,YN,DL,NN(I),ROE)
         M=NN(I)
         PRINT,'NN=',M
         DO 70 J=1,M
 70       PRINT,ROE(J)
         DO 20 J=1,M
           K=L+J
          XS(K)=XN(J)
 20        YS(K)=YN(J)
 10      L=L+NN(I)
C
C  PRINT NODES
C
       PRINT50
       DO 30 I=1,L
        XP(I)=1000.0*XS(I)
        YP(I)=1000.0*YS(I)
 30    PRINT60,XS(I),YS(I)
C
```

```
      CALL TRIANG(NL,NN,IT,NT)
C       CALL MESH(XS,YS,NOD,T,NT)
      CALL DIRI(VDC,NN,NL)
      CALL ALT2(NL,NN,RDC,THS,S1)
       STOP
 50    FORMAT(1X,'NODES')
 60    FORMAT(1X,F19.15,F20.15)
      END
C
C  TAKING THE PATH AND RETURNING THE NODES
C
      SUBROUTINE PATH(TSTEP,NP,TD,NN,XN,YN,TN,DL,RDC,X,Y,T,D,G,I)
C
      IMPLICIT REAL*8 (A-H,O-Z)
      REAL*8 X(28000),Y(28000),D(28000),TD,XN(200),YN(200),R,TEMP,G
      REAL*8 TN(200),TSTEP,T(28000),DL(200)
      INTEGER I,K,NN,NP,NH,J
C
      TEMP=DLOG(1.0+TD*(G-1.0)/(0.3*RDC))/DLOG(G)
      NN=TEMP
      NN=NN+1
      NH=NN/2+1
      XN(1)=X(1)
      YN(1)=Y(1)
      TN(1)=T(1)
      DL(1)=D(1)
      K=2
      TEMP=0.3*RDC
C
      DO 220 J=1,NP
       IF(D(J).LE.TEMP) GOTO 220
       XN(K)=X(J)
       YN(K)=Y(J)
       TN(K)=T(J)
       DL(K)=D(J)
       TEMP=D(J)+(0.3*RDC)*G**(K-1)
       K=K+1
220   CONTINUE
230   CONTINUE
```

```
C
C 235      CONTINUE
C 237      CONTINUE
C
       IF(Y(NP).LT.1.0) Y(NP)=0.0D0
       XN(NN)=X(NP)
       YN(NN)=Y(NP)
       TN(NN)=T(NP)
       DL(NN)=D(NP)
C        NN=NN+1
C       ELSE DO
C        IF(Y(NP).LT.0.0) Y(NP)=0.0D0
C        XN(NN)=X(NP)
C        YN(NN)=Y(NP)
C        TN(NN)=T(NP)
C        DL(NN)=D(NP)
C       END IF
C
      RETURN
      END
C
C DETERMINING THE INITIAL DISTRIBUTION OF THE CHARGE DENSITY
C
      SUBROUTINE INROE(TH,RDC,PI,XN,YN,TN,NN,ROE)
      IMPLICIT REAL*8 (A-H,O-Z)
      REAL*8 XN(200),YN(200),TN(200),ROE(200),EPSO,FK,CI,TH,EST,
     & EON,RDC,T,PI,EEX,EEY
      INTEGER NN,I,J,K
      EPSO=8.854D-12
      FK=1.5D-4
      CI=1.222D-5
     EEX=EX(XN(1),YN(1),0.0D0)
     EEY=EY(XN(1),YN(1),0.0D0)
     EST=DSQRT(EEX**2+EEY**2)
     ROEM=0.236134D-6
C       EON=5.981D+6
C       ROE(1)=CI/(4.0*RDC*FK*EST)*DCOS(TH/2.0*PI/180.0)
      ROE(1)=ROEM*0.5*(1.0+DCOS(TH*PI/180.0))
```

```
C       ROE(1)=ROEM*DCOS(TH/2.0*PI/180.0)
        DO 10 J=2,NN
10      ROE(J)=ROE(1)/(1.0+ROE(1)*FK*TN(J)/EPSO)
        RETURN
        END
C
C
        SUBROUTINE CINROE(TH,RDC,PI,XN,YN,DL,NN,ROE)
        IMPLICIT REAL*8 (A-H,O-Z)
        REAL*8 XN(200),YN(200),DL(200),ROE(200),EPSO,FK,ROEM,TH,
     & EON,RDC,T,PI,FK2,DS(200),EEX,EEY,EST
        INTEGER NN,I,J,K
        EPSO=8.854D-12
        FK=1.5D-4
        EON=2.209D+6
        EEX=EX(XN(1),YN(1),0.0D0)
        EEY=EY(XN(1),YN(1),0.0D0)
        EST=DSQRT(EEX**2+EEY**2)
C       ROEM=0.0714/(FK*EST)
C       PRINT,'ROEM=',ROEM
C       ROEM=0.136134D-06
        ROEM=0.46134D-07
C       ROE(1)=ROEM*DCOS(TH/2.0*PI/180.0)
        ROE(1)=ROEM*0.5*(1.0+DCOS(TH*PI/180.0))
        FK2=DSQRT(RDC*EON*EPSO/ROE(1))
        DO 10 J=2,NN
        DS(J)=DSQRT(XN(J)**2+(16.34-YN(J))**2)
C10     ROE(J)=DSQRT((EPSO*EON*RDC*ROE(1))/(DS(J)**2+FK2**2-RDC**2))
10      ROE(J)=DSQRT((EPSO*EON*RDC*ROE(1))/(DL(J)**2+FK2**2-RDC**2))
        RETURN
        END
C
C DEFINING THE TRIANGLES
C
        SUBROUTINE TRIANG(NL,NN,IT,NT)
C
        IMPLICIT REAL*8 (A-H,O-Z)
        INTEGER IT(800,3),NL,NN(20),NT,I,J,K,L,NL2,NN1,NND
C
```

```
      K=0
      NT=0
      NL1=NL-1
      DO 310 I=1,NL1
       NN1=2*NN(I)-NN(I+1)-1
C
        DO 320 J=1,NN1
C
          IT(NT+1,1)=K+J
          IT(NT+1,2)=K+NN(I)+J
          IT(NT+1,3)=K+NN(I)+J+1
C
          IT(NT+2,1)=K+J
          IT(NT+2,2)=K+NN(I)+J+1
          IT(NT+2,3)=K+J+1
 320        NT=NT+2
C
       K=K+NN(I)
       IF(NN(I+1).EQ.NN(I)) GOTO 310
      NND=IABS(NN(I+1)-NN(I))
C
       DO 330 L=1,NND
        IT(NT+1,1)=K-NND+L-1
        IT(NT+1,2)=K+NN(I)-NND+2*L-2
        IT(NT+1,3)=K+NN(I)-NND+2*L-1
C
        IT(NT+2,1)=K-NND+L-1
        IT(NT+2,2)=K+NN(I)-NND+2*L-1
        IT(NT+2,3)=K-NND+L
C
        IT(NT+3,1)=K+NN(I)-NND+2*L-1
        IT(NT+3,2)=K+NN(I)-NND+2*L
        IT(NT+3,3)=K-NND+L
 330      NT=NT+3
 310   CONTINUE
C
      NT=0
      PRINT370
```

```
      DO 340 I=1,NL1
       NT=NT+(NN(I)-1)*2
 340   NT=NT+NN(I+1)-NN(I)
C
      DO 350 I=1,NT
 350   PRINT 360,IT(I,1),IT(I,2),IT(I,3)
C
      RETURN
 360   FORMAT(1X,I3,2I4)
 370   FORMAT(1X,'TRIANGLES')
      END
C
C  DETERMINING THE PATH OF A PARTICLE USING A RUNGE-KUTTA 4TH ORDER
C
      SUBROUTINE RKP(TH,TSTEP,RDC,NP,TD,X,Y,T,D,TNMIN,TNMAX)
      IMPLICIT REAL*8 (A-H,O-Z)
      REAL*8 H1,H2,W,RDC,TOT,TNMIN,TNMAX,TSTEP,
     & RH,X(28000),Y(28000),T(28000),H,TN1,TH,PI,FK,D(28000),TD,DS,YSTEP
      INTEGER I,J,ND
      COMMON A,B,C,DET,VDC,VAC,PHI,H1,H2,W,H3,S1,S3
C
C
      RAC=0.01599
      RDC=0.01755
      PI=3.141592654
      FK=0.00015
      A=DLOG(2.0*H3/RAC)+0.5*DLOG(((2*S3)**2+RAC**2)/((2*S3)**2
     & +(2*H3)**2))
      B=0.5*DLOG(((S1-S3)**2+(H1+H3)**2)*((S1+S3)**2+(H1-H3)**2)
     & /(((S1-S3)**2+(H1-H3)**2)*((S1+S3)**2+(H1+H3)**2)))
      C=DLOG(2*H1/RDC)+0.5*DLOG(((2*S1)**2+RDC**2)/((2*S1)**2+
     & (2*H1)**2))
      DET=A*C-B**2
      H=FK*TSTEP
C
C  MAXIMUM AND MINIMUM DISTANCES BETWEEN SUCCESIVE POINTS
C
      X(1)=S1+RDC*DSIN(PI*TH/180.0)
      Y(1)=H1-RDC*DCOS(PI*TH/180.0)
```

```
      T(1)=0.0
      D(1)=0.0
C
      DO 110 I=1,28000
C       PRINT,'X=',X(I),'Y=',Y(I),'TN1=',TN1
      RH=DSQRT((Y(I)-H3)**2+(X(I)-S3)**2)
      IF(Y(I).LE.0.0) GOTO 150
 120   CALL RK4(X(I),Y(I),X(I+1),Y(I+1),T(I),H,TN1,FK)
      IF(TN1.LT.TNMAX) GOTO 130
C  DECREASE STEP SIZE
C
      H=H*0.5
      GOTO 120
 130   DS=DSQRT((X(I+1)-X(I))**2+(Y(I+1)-Y(I))**2)
      IF(DS.LT.RDC) GOTO 170
      H=H*0.5
      GOTO 120
C
C  INCREASE STEP SIZE
 170   IF(TN1.GT.TNMIN) GOTO 140
      H=H*2.0
C
C  INCREMENT TIME
C
 140   T(I+1)=T(I)+H/FK
      D(I+1)=D(I)+DS
C
 110  CONTINUE
C
C  HIT
C
 150  NP=I
    TOT=T(NP)
C     PRINT,'TOT=',TOT
    TD=D(NP)
    RETURN
C
    END
```

```
C
C  A SINGLE STEP OF THE R-K METHOD
      SUBROUTINE RK4(XN,YN,XN1,YN1,T,H,TN1,K)
C
      IMPLICIT REAL*8 (A-H,O-Z)
      REAL*8 T,H,XN,YN,XN1,YN1,TN1,KX1,KX2,KX3,KX4,KX5,KX6
      REAL*8 KY1,KY2,KY3,KY4,KY5,KY6,K,TT,XP,YP
C
      KX1=EX(XN,YN,T)
      KY1=EY(XN,YN,T)
C
      XP=XN+H*KX1/2.0
      YP=YN+H*KY1/2.0
      TT=T+H/2.0/K
      KX2=EX(XP,YP,TT)
      KY2=EY(XP,YP,TT)
C
      XP=XN+H*(KX1+KX2)/4.0
      YP=YN+H*(KY1+KY2)/4.0
      TT=T+H/2.0/K
      KX3=EX(XP,YP,TT)
      KY3=EY(XP,YP,TT)
C
      XP=XN-H*KX2+2.0*H*KX3
      YP=YN-H*KY2+2.0*H*KY3
      TT=T+H/K
      KX4=EX(XP,YP,TT)
      KY4=EY(XP,YP,TT)
C
      XP=XN+H*(7.0*KX1+10.0*KX2+KX4)/27.0
      YP=YN+H*(7.0*KY1+10.0*KY2+KY4)/27.0
      TT=T+H/1.5/K
      KX5=EX(XP,YP,TT)
      KY5=EY(XP,YP,TT)
C
      XP=XN+H*(28.0*KX1-125.0*KX2+546.0*KX3+54.0*KX4-378.0*KX5)/625.0
      YP=YN+H*(28.0*KY1-125.0*KY2+546.0*KY3+54.0*KY4-378.0*KY5)/625.0
      TT=T+H/5.0/K
```

```
      KX6=EX(XP,YP,TT)
      KY6=EY(XP,YP,TT)
C
      XN1=XN+H*(KX1+4.0*KX3+KX4)/6.0
      YN1=YN+H*(KY1+4.0*KY3+KY4)/6.0
C
C  CALCULATION OF ESTIMATE OF TRUNCATION ERROR
C
      XP=(-42.0*KX1-224.0*KX3-21.0*KX4+162.0*KX5+125.0*KX6)
      YP=(-42.0*KY1-224.0*KY3-21.0*KY4+162.0*KY5+125.0*KY6)
      TN1=H*DSQRT(XP**2+YP**2)/336.0
C       PRINT,'XN1=',XN1,'YN1=',YN1,'TN1=',TN1
      RETURN
      END
C
C  DETERMINING THE DIRI B.C.
C
      SUBROUTINE DIRI(VDC,NN,NL)
      REAL*8 VDC,V
      INTEGER NN(20),NL,NL1,I,J,N1,N2
      PRINT 630
      NL1=NL-1
      J=0
      DO 620 I=1,NL1
      N1=J+1
      N2=J+NN(I)+1
      PRINT 610,N1,N2,VDC
      J=J+NN(I)
      N2=J+NN(I+1)
      V=0.0D0
 620   PRINT 610, J,N2,V
      RETURN
 610   FORMAT(1X,I3,I4,4X,F10.3)
 630   FORMAT(1X,'DIRI')
      END
C
C  DETERMINING THE CURVED BOUNDARY
C
      SUBROUTINE ALT2(NL,NN,RDC,THS,S1)
```

```
      REAL*8 TH,THS,XA,YA,RDC,S1
      INTEGER NN(20),NL,NL1,I,J,LN
C2      H1=16.34
      H1=17.34
      NL1=NL-1
      PI=3.141592653
      LN=4
      K=1
      PRINT 50
      DO 10 I=1,4
       TH=THS/2.0+(I-1)*THS+63.0
       XA=S1+RDC*DSIN(PI*TH/180.0)
       YA=H1-RDC*DCOS(PI*TH/180.0)
       PRINT 100,K,LN,XA,YA
10     K=I*34+I
50     FORMAT(1X,'ALTERED NODES')
100    FORMAT(1X,I3,I4,4X,2F20.15)
      RETURN
      END
C
C EVALUATING THE FIELD IN THE X DIRECTION AT A GIVEN TIME AND POSITION
C
      FUNCTION EX(X,Y,T)
C
      IMPLICIT REAL*8 (A-H,O-Z)

      COMMON A,B,C,DET,VDC,VAC,H1,H2,W,H3,S1,S3
C
C CALCULATING CHARGE ON CONDUCTORS
C
     Q1=(A*VDC+B*VAC*DSIN(W*T))/DET
     Q3=(-B*VDC+C*VAC*DSIN(W*T))/DET
C
     D1=(X-S1)**2+(Y-H1)**2
     D11=(X-S1)**2+(Y+H1)**2
     D2=(X+S1)**2+(Y-H1)**2
     D21=(X+S1)**2+(Y+H1)**2
     D3=(X-S3)**2+(Y-H3)**2
```

```
      D31=(X-S3)**2+(Y+H3)**2
      D4=(X+S3)**2+(Y-H3)**2
      D41=(X+S3)**2+(Y+H3)**2
C
      EX1=Q1*(X-S1)/D1
      EX11=-Q1*(X-S1)/D11
      EX2=-Q1*(X+S1)/D2
      EX21=Q1*(X+S1)/D21
      EX3=Q3*(X-S3)/D3
      EX31=-Q3*(X-S3)/D31
      EX4=-Q3*(X+S3)/D4
      EX41=Q3*(X+S3)/D41
C
      EX=EX1+EX2+EX3+EX4+EX11+EX21+EX31+EX41
      RETURN
      END
C
C  EVALUATING THE ELECTRIC FIELD IN THE Y DIRECTION FOR A GIVEN TIME
C  AND POSITION
C
      FUNCTION EY(X,Y,T)
C
      IMPLICIT REAL*8(A-H,O-Z)

      COMMON A,B,C,DET,VDC,VAC,H1,H2,W,H3,S1,S3
C
C  CALCULATING CHARGE ON CONDUCTORS
C
     Q1=(A*VDC+B*VAC*DSIN(W*T))/DET
     Q3=(-B*VDC+C*VAC*DSIN(W*T))/DET
C
     D1=(X-S1)**2+(Y-H1)**2
     D11=(X-S1)**2+(Y+H1)**2
     D2=(X+S1)**2+(Y-H1)**2
     D21=(X+S1)**2+(Y+H1)**2
     D3=(X-S3)**2+(Y-H3)**2
     D31=(X-S3)**2+(Y+H3)**2
     D4=(X+S3)**2+(Y-H3)**2
     D41=(X+S3)**2+(Y+H3)**2
```

```
C
      EY1=-Q1*(H1-Y)/D1
      EY11=-Q1*(H1+Y)/D11
      EY2=Q1*(H1-Y)/D2
      EY21=Q1*(H1+Y)/D21
      EY3=-Q3*(H3-Y)/D3
      EY31=-Q3*(H3+Y)/D31
      EY4=Q3*(H3-Y)/D4
      EY41=Q3*(H3+Y)/D41
C
      EY=EY1+EY2+EY3+EY4+EY11+EY21+EY31+EY41
      RETURN
      END
C
$ENTRY
```

B.2 ITERATIVE FINITE ELEMENT PROGRAM

```
//WANG  JOB ',,T=35M,L=50,I=100',CLASS=1
// EXEC WATFIV,SIZE=2000K,P=D
//GO.FT08F001 DD DSN=WANG.ROEAD2,DISP=SHR
//GO.FT09F001 DD DSN=WANG.TRIAD2,DISP=SHR
//GO.FT10F001 DD DSN=WANG.XYAD2,DISP=SHR
//GO.FT11F001 DD DSN=WANG.DIRIAD2,DISP=SHR
//GO.FT12F001 DD DSN=WANG.ALTAD2,DISP=SHR
//GO.FT13F001 DD DSN=WANG.EOUT2,DISP=OLD
//SYSIN DD *
$JOB   WATFIV  WANG,NOEXT
C$OPTIONS TIME=100
C
C
C  THIS IS THE MAIN PROGRAMM FOR HYBRID AC/DC #2 TRANSMISSION LINE
C
      IMPLICIT REAL*8 (A-H,O-Z)
      DOUBLE PRECISION S(60000),X(2000),Y(2000),DIR(2000),B(2000),
     & A1(54),A2(54),A3(54),SUB(5),EPCN(50),ELCN(50),EPGN(50),ELGN(50)
      DOUBLE PRECISION EICN(20),EIG(50),FJ(20),
     & FP(800),FA(800),ROT(800),PEX(800),PEY(800),EX(800),EY(800),
     & XN(800),YN(800),PV(800),VL(800),TNW(800,3),RON(800),XT(800),
     & YT(800),XCN(20),YCN(20),DTRI(800),ROC(20),DV(100),DRO(100),
     & DE(100),EFG(20),XGN(50),YGN(50),VCN(20),VLCN(20),VGN(50),VLGN(50)
      DIMENSION IL1(60000),IL2(60000),IS1(2000),IS2(2000),IS3(2000),
```

```
     & IS4(2000), INODE(6000),IT(800,3)
       COMMON /DATA/ VDC,PI,RAC,RDC,H1,S1,H2,H3,S3,A,B1,C,DET,Q1,Q3
       COMMON /PA/FP,FA
C
       VDC=300000.0
       VAC=0.0
       PI=3.14159265
       FK=1.5D-4
       H1=16.34
       H2=14.20
       H3=12.38
       S1=4.57
       S3=5.49
       RDC=0.01755
       RAC=0.01599
       A=DLOG(2.0*H3/RAC)+0.5*DLOG(((2*S3)**2+RAC**2)/((2*S3)**2
     & +(2*H3)**2))
       B1=0.5*DLOG(((S1-S3)**2+(H1+H3)**2)*((S1+S3)**2+(H1-H3)**2)
     & /(((S1-S3)**2+(H1-H3)**2)*((S1+S3)**2+(H1+H3)**2)))
       C=DLOG(2*H1/RDC)+0.5*DLOG(((2*S1)**2+RDC**2)/((2*S1)**2+
     & (2*H1)**2))
       DET=A*C-B1**2
       Q1=A*VDC/DET
       Q3=-B1*VDC/DET
C
       M=60000
       N=2000
       L=54
```

```
      I=6000
      NT=175
      NNT=115
      NL=5
      NL1=NL-1
C
C
C  INPUT DATA
C  CARD 1
      NDEG=2
      NUNO=115
      NTRI=175
      NF=1
      IPAS=0
      NEIG=0
      NG=0
C
C     CARD 2
      NSOR=0
      NMIX=0
      NDIR=11
      NALT=4
      NFREE=0
      NEQUI=0
      NFILM=0
C
C     CARD 3
```

```
      NGRID=0
      NBOUND=0
      IWRITE=0
      IPRSUP=0
C
C     ONSET ELECTRIC FIELD IN VOLTS/METER
C
      EON=1.84082D+6
      DIFF=1.0D+2
C
      CALL FINP(NT,NNT,NL,NL1,IT,RON,X,Y)
      CALL TDIST(IT,NT,X,Y,TNW)
C       WRITE(13,901)
      WRITE(13,910)
      DO 10 J=1,NT
       XT(J)=(X(IT(J,1))+X(IT(J,2))+X(IT(J,3)))/3.0D0
       YT(J)=(Y(IT(J,1))+Y(IT(J,2))+Y(IT(J,3)))/3.0D0
       ROT(J)=RON(IT(J,1))*TNW(J,1)+RON(IT(J,2))*TNW(J,2)+RON
     & (IT(J,3))*TNW(J,3)
C10      WRITE(13,90) XT(J),YT(J)
 10    WRITE(13,91) ROT(J)
C
C
      WRITE(13,900)
      THM=108.0-66.0
      THS=THM/NL1
      DO 20 J=1,NL
      TH=(J-1)*THS+66.0
```

```
      XCN(J)=RDC*DSIN(PI*TH/180.0)+S1
      YCN(J)=H1-RDC*DCOS(PI*TH/180.0)
20    WRITE(13,90) XCN(J),YCN(J)
      WRITE(13,92)
      NOI=22
      K=NOI
      DO 11 J=1,2
      XGN(J)=X(K)
      YGN(J)=Y(K)
      WRITE(13,90) XGN(J),YGN(J)
11    K=K+NOI
      K=67
      DO 12 J=3,4
      XGN(J)=X(K)
      YGN(J)=Y(K)
      WRITE(13,90) XGN(J),YGN(J)
12    K=K+23
      J=5
      K=115
      XGN(J)=X(K)
      YGN(J)=Y(K)
      WRITE(13,90) XGN(J),YGN(J)
C  CALCULATE E-FIELD BY IMAGE METHOD
C
      WRITE(13,210)
210   FORMAT(1X,'EICN')
      DO 21 J=1,NL1
      EEX=EXI(XCN(J),YCN(J))
```

```
      EEY=EYI(XCN(J),YCN(J))
      EICN(J)=DSQRT(EEX**2+EEY**2)
      WRITE(13,211) EICN(J)
  211  FORMAT(1X,G20.5)
   21  CONTINUE
      WRITE(13,212)
  212  FORMAT(1X,'EIG')
      DO 22 J=1,NL
      EEX=EXI(XGN(J),YGN(J))
      EEY=EYI(XGN(J),YGN(J))
      EIG(J)=DSQRT(EEX**2+EEY**2)
      WRITE(13,213) EIG(J)
   22  CONTINUE
C
C
      NK=30
      DO 30 J=1,NK
CCC       IF(DIFF.LE.1.0D-2) GOTO 200
400       CALL TOP(NT,ROT,RON,TNW,IT)
      CALL MAIND(S,IL1,IL2,X,Y,DIR,B,IS1,IS2,IS3,IS4,A1,A2,A3,INODE,
     & M,N,L,I,IT)
      REWIND 11
      REWIND 12
      CALL PEOUT(X,Y,B,INODE,SUB,PEX,PEY,XN,YN,NNT,J,PV,NT,XT,YT,
     & XCN,YCN,XGN,YGN,EPCN,VCN,NL,EPGN,VGN)
C       CALL EDIFF(NOI,NL1,NNT,XCN,YCN,XGN,YGN,EICN,EIG,
C      & EPCN,PEX,PEY,PV,VCN,
C      & EFG,EDC,EDG,XT,YT,X,Y)
```

```
      CALL PTOL(NT,ROT,RON,TNW,IT)
      CALL MAIND(S,IL1,IL2,X,Y,DIR,B,IS1,IS2,IS3,IS4,A1,A2,A3,INODE,
     & M,N,L,I,IT)
      REWIND 11
      REWIND 12
      CALL LEOUT(X,Y,B,INODE,SUB,EX,EY,XN,YN,NNT,J,VL,NT,XT,YT,
     & XCN,YCN,XGN,YGN,ELCN,VLCN,NL,ELGN,VLGN)
C     CALL EDIFF(NOI,NL1,NT,XCN,YCN,EICN,EIG,ELCN,EX,EY,VL,VLCN,
C    & EFG,EDC,EDG,X,Y,XT,YT)
      CALL NEWROE (NT,NOI,ROT,PEX,PEY,EX,EY,DIFF,NL1,J,EPCN,
     & ELCN,PV,VL,DV,DRO,DE)
C     IF(J.GT.1) THEN DO
C      IF(DRO(J).GT.DRO(J-1)) GOTO 400
C     ELSE DO
C     END IF
30    CONTINUE
200   FJ(1)=FK*ROT(42)*0.5*(EPGN(1)+ELGN(1))
      FJ(2)=FK*(ROT(41)+ROT(42)+ROT(84)+ROT(85))/4.0*0.5*
     & (EPGN(2)+ELGN(2))
      FJ(3)=FK*(ROT(85)+ROT(129))/2.0*0.5*
     & (EPGN(3)+ELGN(3))
      FJ(4)=FK*(ROT(128)+ROT(129)+ROT(174)+ROT(175))/4.0
     & *0.5*(EPGN(4)+ELGN(4))
      FJ(5)=FK*ROT(175)*0.5*(EPGN(5)+ELGN(5))
      DO 60 J=1,NL
60    WRITE(13,70) XGN(J),FJ(J)
      DO 61 J=1,NL
     EGN=0.5*(EPGN(J)+ELGN(J))
```

```
 61    WRITE(13,71) XGN(J),EGN
       STOP
 213   FORMAT(1X,G20.5)
 70    FORMAT(1X,2G20.5)
 71    FORMAT(1X,2G20.5)
 90    FORMAT(1X,2G20.10)
 900   FORMAT(1X,'XCN                YCN')
 901   FORMAT(1X,'XT,  YT')
 91    FORMAT(1X,G20.10)
 92    FORMAT(1X,'XGN                YGN')
 910   FORMAT(1X,'ROT')
       END
C
C
C  READ INITIAL VALUE FOR INITIAL CHARGE DISTRI.,XYCOOD,VERTICES OF
C  TRIANGLES
C
      SUBROUTINE FINP(NT,NNT,NL,NL1,IT,RON,X,Y)
      IMPLICIT REAL*8 (A-H,O-Z)
      REAL*8 RON(800),X(2000),Y(2000),ROC(20)
      INTEGER IT(800,3)
      COMMON /PA/FP,FA
C     WRITE(13,162)
      DO 10 J=1,NNT
      READ(8,*) RON(J)
 10   WRITE(13,161) RON(J)
C     DO 11 J=1,NL
C     READ(1,*) ROC(J)
```

```
C 11   WRITE(13,160) ROC(J)
       DO 20 J=1,NNT
20     READ(10,*) X(J),Y(J)
C20    WRITE(13,170) X(J),Y(J)
       DO 30 J=1,NT
30     READ(9,*) IT(J,1),IT(J,2),IT(J,3)
C30    WRITE(13,180) IT(J,1),IT(J,2),IT(J,3)
       RETURN
160    FORMAT(G20.10)
161    FORMAT(1X,G20.10)
162    FORMAT(1X,'RON')
170    FORMAT(2G20.10)
C180   FORMAT(1X,3I4)
       END
C
C  DETERMINING THE WEIGHT OF EACH OF THE NODES IN
C  FINDING TEH AVERAGE CHARACTERISTICS OF THE TRIANGLES
C
       SUBROUTINE TDIST(IT,NT,X,Y,TNW)
C
       IMPLICIT REAL*8(A-H,O-Z)
       REAL*8 X(2000),Y(2000),TNW(800,3)
       INTEGER IT(800,3)
C
       WRITE(13,11)
       DO 10 J=1,NT
        D12=DSQRT((X(IT(J,1))-X(IT(J,2)))**2+(Y(IT(J,1))-Y
      & (IT(J,2)))**2)
```

```
      D23=DSQRT((X(IT(J,2))-X(IT(J,3)))**2+(Y(IT(J,2))-Y
     & (IT(J,3)))**2)
      D31=DSQRT((X(IT(J,3))-X(IT(J,1)))**2+(Y(IT(J,3))-Y
     & (IT(J,1)))**2)
       DD=D12+D23+D31
       TNW(J,1)=0.5D0*(D12+D31)/DD
       TNW(J,2)=0.5D0*(D12+D23)/DD
10       TNW(J,3)=0.5D0*(D23+D31)/DD
C10      WRITE(13,12) TNW(J,1),TNW(J,2),TNW(J,3)
11   FORMAT(1X,'TNW')
12   FORMAT(1X,3G20.10)
     RETURN
     END
C
C
C    THE CODFFICIENTS OF THE PDE
C
     SUBROUTINE ABC(ITR,FX,FY,A1,B1,C1,D1,E1,P1)
C
     IMPLICIT REAL*8 (A-H,O-Z)
     REAL*8 FP(800),FA(800)
     COMMON /PA/FP,FA
     A1=FA(ITR)
     B1=0.0
     C1=FA(ITR)
     D1=0.0
     P1=FP(ITR)
     RETURN
```

```
      END
C
C
C  CHANGING THE COEFFICIENTS OF THE PDE SO THAT
C  POISSON'S EQUATION IS SOLVED
C
      SUBROUTINE TOP(NT,ROT,RON,TNW,IT)
      IMPLICIT REAL*8 (A-H,O-Z)
      REAL*8 ROT(800),RON(800),FP(800),FA(800),TNW(800,3)
      INTEGER IT(800,3)
       COMMON /PA/FP,FA
      PI=3.141592654
      EPSO=8.854D-12
      DO 10 J=1,NT
      FP(J)=ROT(J)/EPSO
10     FA(J)=1.0D0
      RETURN
      END
C
C
C  CALCULATING THE ELECTRIC FIELD FROM THE SOLUTION
C  OF POISSON'S EQUATION
C
      SUBROUTINE PEOUT(X,Y,B,INODE,SUB,PEX,PEY,XN,YN,NNT,J,PV,NT
     & ,XT,YT,XCN,YCN,XGN,YGN,EPCN,VCN,NL,EPGN,VGN)
      IMPLICIT REAL*8 (A-H,O-Z)
      REAL*8 X(2000),Y(2000),B(2000),SUB(5),PEX(800),PEY(800),PV(800),
     & XN(800),YN(800),XT(800),YT(800),XCN(20),YCN(20),EPCN(20),VCN(20),
```

```
     & VG(50),EPGN(50),VGN(50),XGN(50),YGN(50)
      INTEGER INODE(6000)
C
      WRITE(13,250) J
      DO 10 K=1,NT
CC      XN(K)=X(K)
CC      YN(K)=Y(K)
C      WRITE(13,50) XN(K),YN(K)
     PEX(K)=PHI(XT(K),YT(K),1,X,Y,B,INODE,SUB)
     PEY(K)=PHI(XT(K),YT(K),2,X,Y,B,INODE,SUB)
     PV(K)=PHI(XT(K),YT(K),0,X,Y,B,INODE,SUB)
C      WRITE(13,30) PV(K),VI(XN(K),YN(K))
10    CONTINUE
     NL1=NL-1
     WRITE(13,31)
     DO 20 K=1,NL1
     PEX(800)=PHI(XCN(K),YCN(K),1,X,Y,B,INODE,SUB)
     PEY(800)=PHI(XCN(K),YCN(K),2,X,Y,B,INODE,SUB)
     VCN(K)=PHI(XCN(K),YCN(K),0,X,Y,B,INODE,SUB)
     EPCN(K)=DSQRT(PEX(800)**2+PEY(800)**2)
20    WRITE(13,40) EPCN(K),VCN(K),VI(XCN(K),YCN(K))
     WRITE(13,41)
     DO 21 K=1,NL
     PEX(800)=PHI(XGN(K),YGN(K),1,X,Y,B,INODE,SUB)
     PEY(800)=PHI(XGN(K),YGN(K),2,X,Y,B,INODE,SUB)
     VGN(K)=PHI(XGN(K),YGN(K),0,X,Y,B,INODE,SUB)
     EPGN(K)=DSQRT(PEX(800)**2+PEY(800)**2)
21    WRITE(13,40) EPGN(K),VGN(K),VI(XGN(K),YGN(K))
```

```
30    FORMAT(1X,2G20.5)
31    FORMAT(1X,'EPCN                VCN          VI')
40    FORMAT(1X,3G20.5)
41    FORMAT(1X,'EPGN                VGN          VI')
50    FORMAT(1X,'XN=',G20.5,5X,'YN=',G20.5)
      RETURN
250   FORMAT(1X,'POISSON ELECTRIC FIELD ITERATION #',I3)
      END
C
C
C  PRINTING OUT THE DIFFERENCE OF ELECTROSTATIC E-FIELD
C  AT BOTH CONDUCTOR SURFACE AND THE GROUND LEVEL
C
      SUBROUTINE EDIFF(NOI,NL1,NXY,XCN,YCN,XGN,YGN,EICN,EIG,
     & EPCN,PEX,PEY,PV,
     & VCN,EFG,EDC,EDG,XT,YT,XN,YN)
      IMPLICIT REAL*8 (A-H,O-Z)
      REAL*8 EICN(20),EIG(20),EPCN(20),PEX(800),PEY(800),PV(800),
     & EFG(20),XCN(20),YCN(20),VCN(20),EE(800),EEI(800),XT(800),YT(800),
     & XN(800),YN(800),XGN(20),YGN(20)
      NGR=4
      J1=1
      K1=NOI
      K2=NGR*NOI
      WRITE(13,40)
      DO 10 J=K1,K2,NOI
      EFG(J1)=DSQRT(PEX(J)**2+PEY(J)**2)
      VG(J1)=PV(J)
```

```
      WRITE(13,50) EFG(J1),EIG(J1),VG(J1)
      J1=J1+1
10    CONTINUE
      WRITE(13,100)
      EDC=0.0D0
      VDCN=0.0D0
      DO 20 J=1,NL1
     EDC=EDC+((EICN(J)-EPCN(J))/EICN(J))**2
     VDCN=VDCN+((VCN(J)-VI(XCN(J),YCN(J)))/VI(XCN(J),YCN(J)))**2
20    WRITE(13,200) J,EPCN(J),EICN(J)
      EDC=DSQRT(EDC/NL1)
      VDCN=DSQRT(VDCN/NL1)
      WRITE(13,201) EDC,VDCN
      WRITE(13,300)
      EDG=0.0
      DO 30 J=1,NGR
     EDG=EDG+((EIG(J)-EFG(J))/EIG(J))**2
30    WRITE(13,400) J,EDG
     EDG=DSQRT(EDG/NGR)
      WRITE(13,401) EDG
      VD=0.0D0
      ED=0.0D0
      WRITE(13,11)
      DO 60 J=1,NXY
     EE(J)=DSQRT(PEX(J)**2+PEY(J)**2)
     EEI(J)=DSQRT(EXI(XN(J),YN(J))**2+EYI(XN(J),YN(J))**2)
     ED=ED+((EE(J)-EEI(J))/(0.5*(EE(J)+EEI(J))))**2
```

```
      VD=VD+((PV(J)-VI(XN(J),YN(J)))/(0.5*(VI(XN(J),YN(J))+
     & PV(J)+1.0D-9)))**2
60    WRITE(13,51) EE(J),EEI(J)
      ED=DSQRT(ED/NXY)
      VD=DSQRT(VD/NXY)
      WRITE(13,61) ED,VD
      RETURN
11    FORMAT(1X,'EE              EEI')
40    FORMAT(1X,'   EFG   EIG    VG')
50    FORMAT(1X,3G20.5)
51    FORMAT(1X,2G20.5,G20.10)
61    FORMAT(1X,'ED=',G20.10,'VD=',G20.10)
100   FORMAT(1X,' J,  EPCN    EICN')
200   FORMAT(1X,I3,3X,G20.5,2X,G20.5)
201   FORMAT(1X,'EDC=',G20.10,'VDCN=',G20.10)
300   FORMAT(1X,' J,  EDG')
400   FORMAT(1X,I3,3X,G20.10)
401   FORMAT(1X,'EDG=',G20.10)
      END
C
C
C  CHANGING THE COFFICIENTS OF THE PDE SO THAT THE
C  INHOMOGENOUS EQUATION IS SOLVED
C
      SUBROUTINE PTOL(NT,ROT,RON,TNW,IT)
      IMPLICIT REAL*8 (A-H,O-Z)
      REAL*8 ROT(800),RON(800),FP(800),FA(800),TNW(800,3)
      INTEGER IT(800,3)
```

```
      COMMON /PA/FP,FA
      DO 10 J=1,NT
      FP(J)=0.0D0
10    FA(J)=ROT(J)
      RETURN
      END
C
C  CALCULATING THE ELECTRIC FIELD FROM THE SOLUTION
C  OF INHOMOGENEOUS EQUATION
C
      SUBROUTINE LEOUT(X,Y,B,INODE,SUB,EX,EY,XN,YN,NNT,J,VL,NT
     & ,XT,YT,XCN,YCN,XGN,YGN,ELCN,VLCN,NL,ELGN,VLGN)
      IMPLICIT REAL*8 (A-H,O-Z)
      REAL*8 X(2000),Y(2000),B(2000),SUB(5),EX(800),EY(800),VL(800),
     & XN(800),YN(800),XT(800),YT(800),XCN(20),YCN(20),ELCN(20),VLCN(20)
     & ,ELGN(50),VLGN(50),XGN(50),YGN(50)
      INTEGER INODE(6000)
C
      WRITE(13,250) J
      DO 10 K=1,NT
      EX(K)=PHI(XT(K),YT(K),1,X,Y,B,INODE,SUB)
      EY(K)=PHI(XT(K),YT(K),2,X,Y,B,INODE,SUB)
      VL(K)=PHI(XT(K),YT(K),0,X,Y,B,INODE,SUB)
10    CONTINUE
      NL1=NL-1
      WRITE(13,22)
      DO 20 K=1,NL1
      EX(800)=PHI(XCN(K),YCN(K),1,X,Y,B,INODE,SUB)
```

```
      EY(800)=PHI(XCN(K),YCN(K),2,X,Y,B,INODE,SUB)
      VLCN(K)=PHI(XCN(K),YCN(K),0,X,Y,B,INODE,SUB)
      ELCN(K)=DSQRT(EX(800)**2+EY(800)**2)
20    WRITE(13,30) ELCN(K),VLCN(K)
      WRITE(13,31)
      DO 21 K=1,NL
      EX(800)=PHI(XGN(K),YGN(K),1,X,Y,B,INODE,SUB)
      EY(800)=PHI(XGN(K),YGN(K),2,X,Y,B,INODE,SUB)
      VLGN(K)=PHI(XGN(K),YGN(K),0,X,Y,B,INODE,SUB)
      ELGN(K)=DSQRT(EX(800)**2+EY(800)**2)
21    WRITE(13,30) ELGN(K),VLGN(K)
22    FORMAT(1X,'ELCN                VLCN')
30    FORMAT(1X,2G20.5)
31    FORMAT(1X,'ELGN                VLGN')
      RETURN
250   FORMAT(1X,'LAPLACE ELECTRIC FIELD ITERATION #',I3)
      END
C
C   DEFINING THE B.C.OF THE ARTIFICIAL BOUNDARY
C
      FUNCTION FDIR(IF,ITR,X,Y)
      IMPLICIT REAL*8 (A-H,O-Z)
      COMMON /DATA/ VDC,PI,RAC,RDC,H1,S1,H2,H3,S3,A,B1,C,DET,Q1,Q3
C
      D1=(X-S1)**2+(Y-H1)**2
      D11=(X-S1)**2+(Y+H1)**2
      D2=(X+S1)**2+(Y-H1)**2
      D21=(X+S1)**2+(Y+H1)**2
```

```
      D3=(X-S3)**2+(Y-H3)**2
      D31=(X-S3)**2+(Y+H3)**2
      D4=(X+S3)**2+(Y-H3)**2
      D41=(X+S3)**2+(Y+H3)**2
C
     FDIR=Q1*0.5*DLOG(D11*D2/(D1*D21))+Q3*0.5*DLOG(D31*D4/(D3*D41))
      RETURN
      END
C
      FUNCTION EXI(X,Y)
      IMPLICIT REAL*8(A-H,O-Z)
       COMMON /DATA/ VDC,PI,RAC,RDC,H1,S1,H2,H3,S3,A,B1,C,DET,Q1,Q3
C
      D1=(X-S1)**2+(Y-H1)**2
      D11=(X-S1)**2+(Y+H1)**2
      D2=(X+S1)**2+(Y-H1)**2
      D21=(X+S1)**2+(Y+H1)**2
      D3=(X-S3)**2+(Y-H3)**2
      D31=(X-S3)**2+(Y+H3)**2
      D4=(X+S3)**2+(Y-H3)**2
      D41=(X+S3)**2+(Y+H3)**2
C
      EX1=Q1*(X-S1)/D1
      EX11=-Q1*(X-S1)/D11
      EX2=-Q1*(X+S1)/D2
      EX21=Q1*(X+S1)/D21
      EX3=Q3*(X-S3)/D3
      EX31=-Q3*(X-S3)/D31
```

```
      EX4=-Q3*(X+S3)/D4
      EX41=Q3*(X+S3)/D41
C
      EXI=EX1+EX2+EX3+EX4+EX11+EX21+EX31+EX41
      RETURN
      END
C
      FUNCTION EYI(X,Y)
      IMPLICIT REAL*8(A-H,O-Z)
      COMMON /DATA/ VDC,PI,RAC,RDC,H1,S1,H2,H3,S3,A,B1,C,DET,Q1,Q3
C
      D1=(X-S1)**2+(Y-H1)**2
      D11=(X-S1)**2+(Y+H1)**2
      D2=(X+S1)**2+(Y-H1)**2
      D21=(X+S1)**2+(Y+H1)**2
      D3=(X-S3)**2+(Y-H3)**2
      D31=(X-S3)**2+(Y+H3)**2
      D4=(X+S3)**2+(Y-H3)**2
      D41=(X+S3)**2+(Y+H3)**2
C
      EY1=-Q1*(H1-Y)/D1
      EY11=-Q1*(H1+Y)/D11
      EY2=Q1*(H1-Y)/D2
      EY21=Q1*(H1+Y)/D21
      EY3=-Q3*(H3-Y)/D3
      EY31=-Q3*(H3+Y)/D31
      EY4=Q3*(H3-Y)/D4
      EY41=Q3*(H3+Y)/D41
```

```
C
      EYI=EY1+EY2+EY3+EY4+EY11+EY21+EY31+EY41
C
       RETURN
       END
C
       FUNCTION VI(X,Y)
       IMPLICIT REAL*8 (A-H,O-Z)
        COMMON /DATA/ VDC,PI,RAC,RDC,H1,S1,H2,H3,S3,A,B1,C,DET,Q1,Q3
      D1=(X-S1)**2+(Y-H1)**2
      D11=(X-S1)**2+(Y+H1)**2
      D2=(X+S1)**2+(Y-H1)**2
      D21=(X+S1)**2+(Y+H1)**2
      D3=(X-S3)**2+(Y-H3)**2
      D31=(X-S3)**2+(Y+H3)**2
      D4=(X+S3)**2+(Y-H3)**2
      D41=(X+S3)**2+(Y+H3)**2
C
      VI=Q1*0.5*DLOG(D11*D2/(D1*D21))+Q3*0.5*DLOG(D31*D4/(D3*D41))
       RETURN
       END
C
C   THIS SUBROUTINE UPDATES SPACE CHARGE DISTRIBUTION
C
       SUBROUTINE NEWROE(NT,NOI,ROT,PEX,PEY,EX,EY,DIFF,NL1,J,EPCN,
     & ELCN,PV,VL,DV,DRO,DE)
       IMPLICIT REAL*8 (A-H,O-Z)
      REAL*8 ROT(800),PEX(800),PEY(800),EX(800),EY(800),ROT1(800),
```

```
     & EP(800),E(800),EPCN(20),ELCN(20),PV(800),VL(800),DLON(100),
     & DV(100),DRO(100),DE(100),EDI(800),VDI(800),RDI(800),DPON(100)
      INTEGER NN(20)
      NN(1)=22
      NN(2)=22
      NN(3)=23
      NN(4)=23
      NN(5)=25
      EON=1.84082D+6
      DIFF=0.0
      ARFA=-1.0
      BETA=-0.5
      GAMA=-0.25
      CITA=0.0
      A=2.5D0
C       C=1.0
C       D=1.0
      DV(J)=0.0
      DRO(J)=0.0
      DPON(J)=0.0
      DLON(J)=0.0
      DEM=0.0
      DVM=0.0
      DRM=0.0
      DO 10 J1=1,NT
     DV(J)=DV(J)+((VL(J1)-PV(J1))/(VL(J1)+1.0D-9))**2
      EP(J1)=DSQRT(PEX(J1)**2+PEY(J1)**2)
     E(J1)=DSQRT(EX(J1)**2+EY(J1)**2)
```

```
      ROT1(J1)=ROT(J1)
      EDI(J1)=DABS(EP(J1)-E(J1))/(0.5*(EP(J1)+E(J1)))
      VDI(J1)=DABS(VL(J1)-PV(J1))/(VL(J1)+1.0D-9)
      IF(EDI(J1).GE.DEM) DEM=EDI(J1)
      IF(VDI(J1).GE.DVM) DVM=VDI(J1)
   10 DIFF=DIFF+((E(J1)-EP(J1))/(0.5*(E(J1)+EP(J1))))**2
      DIFF=DSQRT(DIFF/NT)
      DV(J)=DSQRT(DV(J)/NT)
      DE(J)=DIFF
      K=0
      DO 20 J1=1,NL1
      DPON(J)=DPON(J)+((EON-EPCN(J1))/EON)**2
      DLON(J)=DLON(J)+((EON-ELCN(J1))/EON)**2
      K1=NN(J1)+NN(J1+1)-2
      DO 30 J2=1,K1
      K=K+1
C     PRINT,'ROT=',ROT(J2),'ROT1=',ROT1(J2)
C     PRINT,'EPCN=',EPCN(J1),'ELCN=',ELCN(J1)
C
      ROT(K)=ROT1(K)
     & *(1.0+ARFA*(EP(K)-E(K))/(EP(K)+E(K)))**A
     & *(1.0+CITA*(PV(K)-VL(K))/(PV(K)+VL(K)))
     & *((1.0+BETA*(EON-EPCN(J1))/EON)
     & *(1.0+GAMA*(EON-ELCN(J1))/EON))
     & **(FLOAT(K1-J2)/FLOAT(K1)/20.0)
C
C5    ROT(K)=ROT1(K)*(0.5*(EPCN(J1)+ELCN(J1))/EON)**A
C5   & *(1.0+ARFA*(EP(K)-E(K))/(EP(K)+E(K)))
```

```
C5    & *(1.0+GAMA*(PV(K)-VL(K))/(PV(K)+VL(K)))
 30   CONTINUE
 20   CONTINUE
      DPON(J)=DSQRT(DPON(J)/NL1)
      DLON(J)=DSQRT(DLON(J)/NL1)
C      WRITE (13,41)
      DO 40 J1=1,NT
      DRO(J)=DRO(J)+((ROT(J1)-ROT1(J1))/ROT1(J1))**2
      RDI(J1)=DABS(ROT(J1)-ROT1(J1))/ROT1(J1)
      IF(RDI(J1).GE.DRM) DRM=RDI(J1)
C      WRITE(13,50) J1,ROT(J1),ROT1(J1),PV(J1),VL(J1),EP(J1),E(J1)
 40   CONTINUE
      DRO(J)=DSQRT(DRO(J)/NT)
      WRITE(13,60) J,DV(J),DRO(J),DE(J)
      WRITE(13,61) DVM,DEM,DRM
      WRITE(13,70) J,DPON(J),DLON(J)
      IF(J.GT.1) THEN DO
       IF(DRO(J).GT.DRO(J-1)) THEN DO
CC          ARFA=1.02*ARFA
CC         BETA=1.02*BETA
CC          GAMA=GAMA+0.5
       ELSE DO
       END IF
      ELSE DO
      END IF
C      PRINT,'GAMA=',GAMA,'J=',J
      RETURN
 41   FORMAT(1X,'# OF ELEMENT  ',7X,'ROT',10X,'ROT1',10X,'PV',/2X,'V',
```

```
     & 10X,'PE',10X,'E')
  50   FORMAT(1X,I3,2(1X,E12.5),1X,F10.2,/1X,1X,F10.2,2(2X,G20.5))
  60   FORMAT(1X,'ITERATION #  ',I3,3X,'DV=',E12.5,/1X,'DROE=',E12.5,1X,
     & 'DE=',E12.5)
  61   FORMAT(1X,'DVM=',G20.10,'DEM=',G20.10,'DRM=',G20.10)
  70   FORMAT(1X,'ITER. #=',I3,'DPEON=',G20.10,'DLEON=',G20.10)
       END
```